rickets, although metaphyseal dysplasia must be ruled out. The main causes of rickets are vitamin D deficiency and hereditary hypophosphatemic rickets. Hypophosphatemia and elevated levels of alkaline phosphatase (ALP) are associated with both vitamin D-deficient and hereditary hypophosphatemic rickets.

Hereditary hypophosphatemic rickets is classified mainly into 4 entities based on mode of inheritance and urinary excretion of calcium (1, 2). Recently, the genes responsible for these forms of hereditary hypophosphatemic rickets have been identified. Autosomal dominant hypophosphatemic rickets (ADHR, MIM 193100) is a rare disease characterized by low levels of serum phosphate and elevated levels of ALP and phosphaturia and is inherited in an autosomal dominant fashion. In 2000, genetic analysis of families with the disease successfully identified that the *FGF23* (fibroblast growth factor 23) gene is responsible for the disease (3). Now FGF23 is recognized as a hormone that plays a central part in regulation of the serum phosphate concentration, and its abnormality is involved in many cases of hypophosphatemic rickets (4, 5). In ADHR, since the mutant FGF23 is resistant to degradation, its concentration is elevated in serum. Thus, this mutation is a gain-of-function type. FGF23 works as a phosphaturic factor after binding to FGFR1 and its co-receptor, klotho, in the kidney and reduces serum phosphate concentrations (6). In addition, FGF23 decreases the production of 1, 25-dihydroxyvitamin D [1,25$(OH)_2$D] in renal tubules (7). In turn, 1, 25$(OH)_2$D and phosphate increase the expression of FGF23 (8). Therefore, administration of active vitamin D and phosphate may exert biphasic effects, i.e., acute increase in phosphate levels followed by decrease in phosphate levels associated with an increase in FGF23 levels.

Autosomal recessive hypophosphatemic rickets (ARHR1, MIM 241520) is also a rare disease in which hypophosphatemia and rickets are observed. The causal gene is *DMP1* (dentine matrix protein 1), and its expression is observed in osteocytes and osteoblasts (9). *ENPP1* is a newly identified causal gene (ARHR2, MIM 613312) (10, 11). The *ENPP1* gene encodes ectonucleotide pyrophosphatase/phosphodiesterase 1 and is also responsible for generalized arterial calcification of infancy (12). Although the mechanism remains obscure, FGF23 is elevated in both types of ARHR and reduces serum phosphate concentrations (13). In Japan, two single families are reported to have abnormalities in each of these gene (14, 15).

Hereditary hypophosphatemic rickets with hypercalciuria (HHRH, MIM 241530) is a rare autosomal recessive disease characterized by hypophosphatemia and hypercalciuria. It is caused by *SLC34A3*, which encodes the type IIc sodium-dependent phosphate co-transporter (NaPi-IIc), a transporter for reabsorption of phosphate in the proximal renal tubules (16–18). The administration of phosphate alone ameliorates hypophosphatemia and hypercalciuria in HHRH.

X-linked hypophosphatemic rickets (XLH, MIM 307800) is the most frequent and prototype form of hypophosphatemic rickets in pediatric practice. In 1995, the gene responsible for the disease was identified as *PHEX* (phosphate regulating gene with homologies to endopeptidases on the X chromosome) (19). To date, over 200 mutations have been found in the *PHEX* gene and listed in the PHEXdb, PHEX Locus Database (http://www.phexdb.mcgill.ca). Patients with XLH are treated with active vitamin D and phosphate buffer. However, phosphate buffer is not available as a prescribed medicine in Japan. In addition, treatment with vitamin D and phosphate buffer is not an absolute cure for the disease, though a recommendation for treatment has been published (20).

Hypophosphatemic rickets is also caused by impaired function of renal tubules and tumors that produce FGF23. Malfunction of renal tubules sometimes involves reabsorption of essential nutrients or minerals other than phosphate and is called Fanconi syndrome (MIM 134600, 613388, or acquired). The acquired form

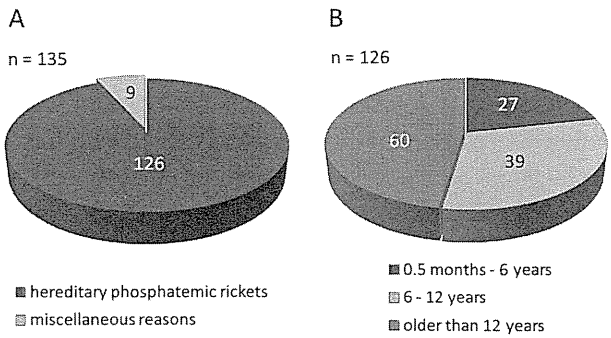

Fig. 1 Patient background. (A) The cause of hypophosphatemia in all patients. (B) The ages of the patients with hereditary hypophosphatemic rickets.

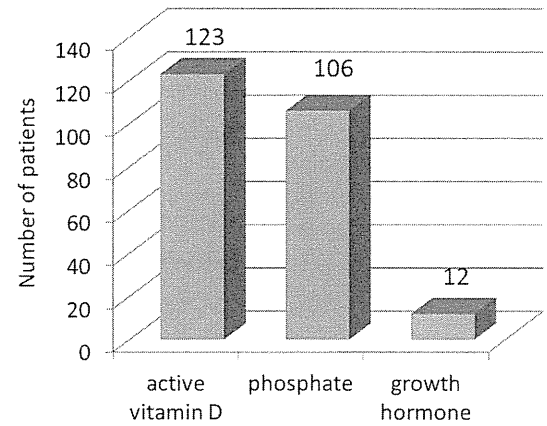

Fig. 2 Treatment for patients with hereditary hypophosphatemic rickets.

is called tumor-induced osteomalacia (TIO) and is rare in childhood (21–23).

We attempted to clarify how hypophosphatemic rickets is actually treated in Japan. To this end, we sent questionnaires concerning the experience of treatment of patients with hypophosphatemic rickets and the actual procedures.

Material and Methods

We sent questionnaires by mail to 68 hospitals where 80 pediatric endocrinologists approved by the Japanese Society of Pediatric Endocrinology worked in 2010. Survey subjects are patients who show hypophosphatemia for more than 6 mo. The questionnaire includes the number patients, patient profiles such as age and sex, hereditary pattern, type of medicine, and dose of phosphate including minimum and maximum dose and frequency.

Results

Responses to the questionnaire were obtained from 53 out of 68 (78% of total) hospitals to which the questionnaires were sent. A total of 135 patients were treated in 28 (53% of response) hospitals during November 2009 and May 2010; 126 patients suffered from hereditary phosphatemic rickets, and 9 had hypophosphatemia caused by other miscellaneous reasons (Fig. 1-A). In this paper, we focused on the 126 patients who had hereditary hypophosphatemic rickets. Patient profiles were as follows: 27 (21%) patients were between 6 mo and 6 yr of age, 39 (31%) patients were between 6 and 12 yr of age, and 60 (48%) patients were more than 12 yr of age (Fig. 1-B). Active vitamin D and phosphate were administered to 123 and 106 patients, respectively. Twelve patients were treated with growth hormone (Fig. 2). The means of the minimum and maximum doses of phosphorus were 37.2 and 58.1 mg/kg/d, respectively, and the dosed were administered in 2 to 6 aliquots (Table 1). Efficacy of the treatment was monitored by various factors including serum phosphate, ALP, intact PTH, urinary Ca/Cr, radiologic features, and growth. In particular, serum phosphate levels were monitored by 18 physicians. The target levels were set between 2 and 3.5 mg/dl. Serum ALP was also used as a marker by 17 physicians. The target levels varied from normal to 2,000 IU/l. In addition, 7 physicians employed intact PTH with target levels varying from normal to twice the normal level.

Table 1 Phosphorus dose and dose frequency

Dose (mg/kg/d)

	Minimum dose	Maximum dose
Mean	37.2	58.1
Range	15–100	30–120

Dose frequency

Physicians that adjust dose frequency: 17

	2 times/d	3 times/d	4 times/d	5 times/d	6 times/d
Minimum	3	9	4	1	–
Maximum	–	1	10	2	4

Physicians that use a fixed frequency: 7

2 times/d	3 times/d	4 times/d	5 times/d	6 times/d
1	–	5	–	1

Discussion

Hereditary hypophosphatemic rickets is often associated with bone deformity, bone pain and growth retardation. Bone deformity sometimes requires surgery for correction. At present, there is no curative therapy for XLH, and active vitamin D and phosphate are administered to correct hypophosphatemia and elevation of ALP (24). However, normalization of the serum phosphate concentration is difficult due to elevation of FGF23, leading to increased excretion of phosphate into urine (25, 26). Insufficient treatment is associated with growth retardation (27). On the other hand, overtreatment with phosphate leads to secondary hyperparathyroidism, and large doses of active vitamin D increase the risk of hypercalciuria (20). Though a recommendation for XLH treatment has been published, it is far from complete cure. Moreover, since phosphate is not a prescribed medicine in Japan, the buffer has to be prepared in the hospital dispensary.

To understand the situation concerning treatment of patients with hereditary hypophosphatemic rickets in Japan, we conducted a questionnaire survey among pediatric endocrinologists. The percentage of the patients with XLH covered by this questionnaire is unclear, but in Japan, it is rare that pediatric nephrologists alone treat patients with XLH.

In the survey, 103 to 106 (82 to 84%) of 123 patients with hereditary hypophosphatemic rickets were treated with both active vitamin D and phosphate. At least 17 (13%) of the patients with hereditary hypophosphatemic rickets were treated with active vitamin D only. Twelve (10%) of the patients with hereditary hypophosphatemic rickets were treated with growth hormone, probably because they had short stature and growth hormone deficiency. The criteria for adjusting the dose of active vitamin D or phosphate buffer were various. One problem is that both serum phosphate and ALP values are age dependent, and normalization of serum phosphate levels and ALP was difficult. X-ray findings are not quantitative, and growth is long term. Thus, these indices are difficult to use in the short term. It is also critical to avoid side effects of the treatment. Thus, the doses of active vitamin D and phosphate should be reduced when hypercalciuria and secondary hyperparathyroidism are observed, respectively.

No information is available concerning the most effective dose of phosphate and how many times it should be administered in the treatment

of patients with hypophosphatemic rickets. In Pediatric Endocrinology and Inborn Errors of Metabolism (28), 40–100 mg/kg/d, divided into 4 to 6 doses, is recommended. However, adherence tends to become poor when short intervals are selected. In this survey, 37.2–58.1 mg/kg/d of phosphorus divided into 3 to 4 doses was most common. Thus, most physicians seemed to treat XLH patients within the recommended way of treatment in the actual clinical setting.

Acknowledgement

We are grateful to all the doctors who responded to the questionnaire.

References

1. Alizadeh Naderi AS, Reilly RF. Hereditary disorders of renal phosphate wasting. Nat Rev Nephrol 2010;6:657–65.
2. Carpenter TO. The expanding family of hypophosphatemic syndromes. J Bone Miner Metab 2012;30:1–9.
3. The ADHR Consortium. Autosomal dominant hypophosphataemic rickets is associated with mutations in *FGF23*. Nat Genet 2000;26:345–8.
4. Yamazaki Y, Okazaki R, Shibata M, Hasegawa Y, Satoh K, Tajima T, *et al.* Increased circulatory level of biologically active full-length FGF-23 in patients with hypophosphatemic rickets/ osteomalacia. J Clin Endocrinol Metab 2002;87:4957–60.
5. White KE, Carn G, Lorenz-Depiereux B, Benet-Pages A, Strom TM, Econs MJ. Autosomal-dominant hypophosphatemic rickets (ADHR) mutations stabilize FGF-23. Kidney Int 2001;60:2079–86.
6. Gattineni J, Baum M. Regulation of phosphate transport by fibroblast growth factor 23 (FGF23): implications for disorders of phosphate metabolism. Pediatr Nephrol 2010;25:591–601.
7. Perwad F, Portale AA. Vitamin D metabolism in the kidney: regulation by phosphorus and fibroblast growth factor 23. Mol Cell Endocrinol 2011;347:17–24.
8. Mirams M, Robinson BG, Mason RS, Nelson AE. Bone as a source of FGF23: regulation by phosphate? Bone 2004;35:1192–9.
9. Feng JQ, Ward LM, Liu S, Lu Y, Xie Y, Yuan B, *et al.* Loss of DMP1 causes rickets and osteomalacia and identifies a role for osteocytes in mineral metabolism. Nat Genet 2006;38:1310–5.
10. Levy-Litan V, Hershkovitz E, Avizov L, Leventhal N, Bercovich D, Chalifa-Caspi V, *et al.* Autosomal-recessive hypophosphatemic rickets is associated with an inactivation mutation in the *ENPP1* gene. Am J Hum Genet 2010;86:273–8.
11. Lorenz-Depiereux B, Schnabel D, Tiosano D, Häusler G, Strom TM. Loss-of-function *ENPP1* mutations cause both generalized arterial calcification of infancy and autosomal-recessive hypophosphatemic rickets. Am J Hum Genet 2010;86:267–72.
12. Rutsch F, Ruf N, Vaingankar S, Toliat MR, Suk A, Höhne W, *et al.* Mutations in *ENPP1* are associated with 'idiopathic' infantile arterial calcification. Nat Genet 2003;34:379–81.
13. Martin A, Liu S, David V, Li H, Karydis A, Feng JQ, *et al.* Bone proteins PHEX and DMP1 regulate fibroblastic growth factor Fgf23 expression in osteocytes through a common pathway involving FGF receptor (FGFR) signaling. FASEB J 2011;25:2551–62.
14. Koshida R, Yamaguchi H, Yamasaki K, Tsuchimochi W, Yonekawa T, Nakazato M. A novel nonsense mutation in the DMP1 gene in a Japanese family with autosomal recessive hypophosphatemic rickets. J Bone Miner Metab 2010;28:585–90.
15. Saito T, Nishii Y, Yasuda T, Ito N, Suzuki H, Igarashi T, *et al.* Familial hypophosphatemic rickets caused by a large deletion in PHEX gene. Eur J Endocrinol 2009;161:647–51.
16. Segawa H, Kaneko I, Takahashi A, Kuwahata M, Ito M, Ohkido I, *et al.* Growth-related renal type II Na/Pi cotransporter. J Biol Chem 2002;277:19665–72.
17. Lorenz-Depiereux B, Benet-Pages A, Eckstein G, Tenenbaum-Rakover Y, Wagenstaller J, Tiosano D, *et al.* Hereditary Hypophosphatemic Rickets with Hypercalciuria is Caused by Mutations in the Sodium-Phosphate Cotransporter Gene *SLC34A3*. Am J Hum Genet 2006;78:193–201.
18. Bergwitz C, Roslin NM, Tieder M, Loredo-Osti

JC, Bastepe M, Abu-Zahra H, *et al. SLC34A3* Mutations in Patients with Hereditary Hypophosphatemic Rickets with Hypercalciuria Predict a Key Role for the Sodium-Phosphate Cotransporter NaPi-IIc in Maintaining Phosphate Homeostasis. Am J Hum Genet 2006;78:179–92.

19. Francis F, Hennig S, Korn B, Reinhardt R, Jong PD, Poustka A, *et al.* A gene (*PEX*) with homologies to endopeptidases is mutated in patients with X-linked hypophosphatemic rickets. Nat Genet 1995;11:130–6.
20. Carpenter TO, Imel EA, Holm IA, Jan de Beur SM, Insogna KL. A clinician's guide to X-linked hypophosphatemia. J Bone Miner Res 2011;26:1381–8.
21. Shimada T, Mizutani S, Muto T, Yoneya T, Hino R, Takeda S, *et al.* Cloning and characterization of FGF23 as a causative factor of tumor-induced osteomalacia. Proc Natl Acad Sci USA 2001;98:6500–5.
22. Jonsson KB, Zahradnik R, Larsson T, White KE, Sugimoto T, Imanishi Y, *et al.* Fibroblast growth factor 23 in oncogenic osteomalacia and X-linked hypophosphatemia. N Engl J Med 2003;348:1656–63.
23. Chong WH, Molinolo AA, Chen CC, Collins MT. Tumor-induced osteomalacia. Endocrine-Related Cancer 2011;18:R53–77.
24. Kienitz T, Ventz M, Kaminsky E, Quinkler M. Novel PHEX nonsense mutation in a patient with X-linked hypophosphatemic rickets and review of current therapeutic regimens. Exp Clin Endocrinol Diabetes 2011;119:431–5.
25. Imel EA, DiMeglio LA, Hui SL, Carpenter TO, Econs MJ. Treatment of X-linked hypophosphatemia with calcitriol and phosphate increases circulating fibroblast growth factor 23 concentrations. J Clin Endocrinol Metab 2010;95:1846–50.
26. Carpenter TO, Insogna KL, Zhang JH, Ellis B, Nieman S, Simpson C, *et al.* Circulating levels of soluble klotho and FGF23 in X-linked hypophosphatemia: circadian variance, effects of treatment, and relationship to parathyroid status. J Clin Endocrinol Metab 2010;95:E352–7.
27. Quinlan C, Guegan K, Offiah A, Neill RO, Hiorns MP, Ellard S, *et al.* Growth in PHEX-associated X-linked hypophosphatemic rickets: the importance of early treatment. Pediatr Nephrol 2012;27:581–8.
28. Roth KS, Ward RJ, Chan JC, Sarafoglou K. Disorders of Calcium, Phosphate, and Bone Metabolism. In: Sarafoglou K, Hoffmann GF, Roth KS, editors. Pediatric Endocrinology and Inborn Errors of Metabolism. New York: McGraw Hill;2009.p.619–64.

THE JOURNAL OF BIOLOGICAL CHEMISTRY VOL. 287, NO. 19, pp. 15760–15775, May 4, 2012

Vinculin Functions as Regulator of Chondrogenesis*■

Received for publication, September 26, 2011, and in revised form, February 21, 2012 Published, JBC Papers in Press, March 13, 2012, DOI 10.1074/jbc.M111.308072

Takao Koshimizu[‡§], Masanobu Kawai[‡], Hiroki Kondou[‡], Kanako Tachikawa[‡], Norio Sakai[¶], Keiichi Ozono[¶], and Toshimi Michigami[‡1]

From the [‡]Department of Bone and Mineral Research, Osaka Medical Center and Research Institute for Maternal and Child Health, 840 Murodo-cho, Izumi, Osaka 594-1101, Japan and the Departments of [¶]Pediatrics and [§]Pediatric and Neonatal-Perinatal Research, Osaka University Graduate School of Medicine, 2-2 Yamada-oka, Suita, Osaka 565-0871, Japan

Background: Vinculin plays profound roles in cell adhesion and migration.
Results: Trapping or knockdown of the vinculin gene in chondrocytes leads to impaired differentiation by affecting multiple signaling pathways.
Conclusion: Vinculin has pleiotropic roles in chondrocytic differentiation.
Significance: This study reveals a novel, tissue-specific function of vinculin in chondrocytes.

To identify the genes involved in chondrocytic differentiation, we applied gene trap mutagenesis to a murine mesenchymal chondrogenic cell line ATDC5 and isolated a clone in which the gene encoding vinculin was trapped. The trapped allele was assumed to express a fusion protein containing a truncated vinculin lacking the tail domain and the *geo* product derived from the trap vector. The truncated vinculin was suggested to exert a dominant negative effect. Impaired functioning of vinculin caused by gene trapping in ATDC5 cells or knockdown in primary chondrocytes resulted in the reduced expression of chondrocyte-specific genes, including *Col2a1*, aggrecan, and *Col10a1*. The expression of *Runx2* also was suppressed by the dysfunctional vinculin. On the other hand, the expression of *Sox9*, encoding a key transcription factor for chondrogenesis, was retained. Knockdown of vinculin in metatarsal organ cultures impaired the growth of the explants and reduced the expression of *Col2a1* and aggrecan. Gene trapping or knockdown of vinculin decreased the phosphorylation of ERK1/2 but increased that of Src homology 2 domain-containing tyrosine phosphatase 2 (SHP2) and Akt during chondrocytic differentiation, suggesting a disturbance of signaling by insulin-like growth factor I (IGF-I). Knockdown of vinculin in the metatarsal organ culture abrogated the IGF-I-induced growth and inhibited the up-regulation of *Col2a1* and aggrecan expression by IGF-I. Loss of vinculin function in differentiating chondrocytes impaired the activation of the p38 MAPK pathway also, suggesting its involvement in the regulation of chondrogenesis by vinculin. Our results indicate a tissue-specific function of vinculin in cartilage whereby it controls chondrocytic differentiation.

Endochondral bone formation consists of the mesenchymal condensation of undifferentiated cells, the proliferation of chondrocytes, and differentiation into hypertrophic chondrocytes, followed by mineralization. Proliferating chondrocytes express type II, IX, and XI collagen and proteoglycans, such as aggrecan, whereas hypertrophic chondrocytes are characterized by a high level of alkaline phosphatase and the production of type X collagen. Various transcription factors and signaling molecules, including Sox9/5/6, Runx2, Indian hedgehog (Ihh), parathyroid hormone-related protein, insulin-like growth factors (IGFs), and fibroblast growth factors (FGFs), have been revealed to regulate the maturation of chondrocytes (1, 2). However, the molecular mechanisms underlying chondrogenesis have not been fully elucidated.

Gene trapping is a genome-wide approach used to clarify the roles of genes by the random insertion of a trapping vector that might disturb gene function (3). A gene trap vector consists of a promoterless reporter gene, a selectable marker, and a splice acceptor site immediately upstream of the reporter gene. When the vector is appropriately inserted in an endogenous gene, a fusion transcript, including the upstream coding sequence of the gene and the reporter gene, is generated by the promoter and enhancer of the trapped gene. This event is associated with the conversion of the trapped gene into a mutated gene and allows one to examine its expression via the reporter activity.

To identify the factors involved in chondrogenesis, we used a gene trap approach in the murine mesenchymal cell line ATDC5, an established cell model of endochondral bone formation (4). ATDC5 cells differentiate into proliferating chondrocytes and undergo cellular hypertrophy and mineralization. By applying gene trapping in ATDC5 cells, we have previously identified several factors involved in chondrocytic differentiation, including the p85a subunit of phosphatidylinositide 3-kinase (PI3K) and nuclear factor I transcription/replication factor (5, 6).

Vinculin is a 116-kDa cytoskeletal protein associated with focal adhesion and adherens junctions. It exists in multimolecular complexes, which function in adhesion and/or signaling between the extracellular milieu and the cell, via integrins and cadherins. The amino-terminal head domain of vinculin binds to talin (7), which in turn binds to β integrins, whereas the carboxyl-terminal tail domain binds to actin (8), phospholipids (9), and paxillin (10). This arrangement allows vinculin to function as a regulatory bridge between the extracellular matrix

* This work was supported in part by Grants-in-aid for Scientific Research from the Ministry of Education, Science, and Culture of Japan (to T. M.) and a grant from the Foundation of Growth Science (to T. M.).
■ This article contains supplemental Table S1 and Figs. S1–S6.
[1] To whom correspondence should be addressed. Tel.: 81-725-56-1220; Fax: 81-725-57-3021; E-mail: michigami@mch.pref.osaka.jp.

(ECM)[2] and the actin cytoskeleton. Disruption of vinculin expression in mice results in embryonic death with severe defects in cardiac and brain development (11, 12). Cells depleted of vinculin have a reduced ability to adhere to a variety of ECM proteins, increased migration rates, and fewer and smaller adhesion sites compared with wild-type cells (12–14). In addition to the profound roles of vinculin in cell adhesion and motility, there might be some tissue-specific functions, which remain to be elucidated.

By gene trapping in chondrocytic ATDC5 cells, we isolated a clone in which the gene encoding vinculin was trapped. The clone expressed a truncated vinculin lacking the tail domain, which exerted a dominant effect. The clone's ability to differentiate into mature chondrocytes was impaired, leading us to hypothesize that vinculin plays a role in chondrocyte differentiation. Here we provide evidence for chondrocyte-specific roles of vinculin and describe possible molecular mechanisms by which vinculin regulates chondrocytic differentiation.

EXPERIMENTAL PROCEDURES

Cell Culture—ATDC5 cells and the trap clones were maintained in a 1:1 mixture of Dulbecco's modified Eagle's and Ham's F-12 (DMEM/F-12) medium (Sigma-Aldrich) supplemented with 5% fetal bovine serum (FBS) (Invitrogen) and 1% insulin-transferrin-selenium G supplement (ITS) (Invitrogen) at 37 °C in a 5% CO_2 atmosphere. For chondrogenic induction, cells were inoculated into 6-well culture plates (5×10^4 cells/well). Three days later, the medium was changed to α-minimal essential medium supplemented with 5% FBS and ITS, and the culture plates were sealed to facilitate mineralization, as described previously (5, 6). The medium was replaced every 3 days.

COS7 cells were cultured in DMEM supplemented with 10% FBS. For transient transfections, FuGene6 reagent (Roche Applied Science) was utilized.

Isolation of Primary Chondrocytes—Animal protocols were approved by the Institutional Animal Care and Use Committee. Primary chondrocytes were isolated from the ribcages of 5-day-old ICR mice following a previous report (15). In brief, the cartilage dissected from ribcages was incubated with actinase E (2 mg/ml in PBS; Kaken Pharmaceutical Co. Ltd., Tokyo, Japan) for 30 min at 37 °C, rinsed three times with PBS, treated with collagenase (3 mg/ml, Wako, Osaka, Japan) in 10 ml of DMEM for 90 min at 37 °C, and then transferred to a 50-ml tube. After pipetting, the tube was stood for 5 min, and the supernatant containing soft tissue was discarded. The remaining cell clumps were washed and passed through a 100-μm cell strainer. The collected chondrocytes were cultured in DMEM supplemented with 10% FBS and 50 μg/ml ascorbic acid (Sigma-Aldrich).

Organ Culture of Mouse Metatarsals—The organ culture of mouse metatarsals was performed following a previous report (16). The central metatarsal rudiments were dissected from each hind limb of E15.5 ICR mouse embryos, placed into 48-well plates (designated day 0), and cultured in α-minimal essential medium containing 50 μg/ml ascorbic acid, 1 mM β-glycerophosphate, 0.2% bovine serum albumin, and 0.1% penicillin/streptomycin at 37 °C under a 5% CO_2 atmosphere. The medium was changed on day 2 and day 4. When viral transfection was performed, the viruses were added to the medium on day 0 and when the medium was changed.

Gene Trapping—As the trap vector, we used pPT1-geo, which lacks its own promoter and enhancer but contains a *lacZ* gene as a reporter fused to a neomycin resistance gene as a selection marker, which was designated *geo* (17). After pPT1-geo was introduced into ATDC5 cells using the Gene Pulser II electroporation system (Bio-Rad), neomycin-resistant clones were selected and screened for β-galactosidase activity. Clones with a 10-fold higher level of β-galactosidase activity than the parental ATDC5 cells were then subjected to chondrogenic induction, followed by Alcian blue and Alizarin red staining to evaluate the production and mineralization of extracellular matrices, respectively.

Cell Staining—The cells were fixed with 95% ethanol and stained with 1% Alizarin red S (Sigma-Aldrich), Alcian blue stain solution, pH 2.5 (Nacalai Tesque, Kyoto, Japan), or 0.1% crystal violet solution (Kanto Chemical, Tokyo, Japan). Staining for β-galactosidase activity was performed using 5-bromo-4-chloro-3-indolyl-β-D-galactopyranoside (X-gal) (Wako) as a substrate.

Southern Blot Analysis—Genomic DNA was extracted from parental ATDC5 cells and the trap clone and digested with the restriction enzyme SphI or PstI. The digested DNA was then electrophoresed, transferred to a Hybond-N^+ membrane (Amersham Biosciences), and probed with a radiolabeled fragment of *lacZ* cDNA prepared by digestion of pPT1-geo with EcoRI/SacI. The restriction enzymes were purchased from New England Biolabs (Beverly, MA).

Identification of Trapped Genes by 5′-Rapid Amplification of cDNA Ends (RACE)—Total RNA was extracted from the trap clone with the RNeasy kit (Qiagen Inc., Valencia, CA), and messenger RNA was purified with oligo(dT) latex (Oligotex™-dT30 Super mRNA Purification Kit; Takara Biomedicals, Shiga, Japan). To identify the trapped gene, 5′-RACE was performed utilizing the 5′-RACE System for Rapid Amplification of cDNA Ends (Invitrogen), according to the manufacturer's instructions with some modifications. Briefly, first-strand cDNA was synthesized from mRNA (1 μg) using SuperScript II reverse transcriptase (Invitrogen) with a primer specific to *lacZ* cDNA in pPT1-geo: LacZ-GSP1, 5′-TGGCGAAAGGGGGATGTG-3′. After the first strand of cDNA was synthesized, the original mRNA template was removed by treatment with RNase, and the unincorporated dNTPs and the primer were separated from the cDNA using a GlassMAX Spin Cartridge (Invitrogen). Then a homopolymeric tail was added to the 3′-end of the cDNA using TdT and dCTP. This was followed by PCR amplification using *Taq* polymerase (Takara) and the following set of primers: 5′-RACE Abridged Anchor Primer, 5′-GGCCACGCGTCGACTAGTACGGGIIGGGIIGGGIIG-3′ (where I represents inosine); LacZ-GSP2, 5′-ATGTGCTGCAAGGCGATTAAGTTG-3′. The product served as the template for a second round

[2] The abbreviations used are: ECM, extracellular matrix; IGF, insulin-like growth factor; FN, fibronectin; Col II, type II collagen; miRNA, microRNA; FAK, focal adhesion kinase; Vh, vinculin head domain; Vt, vinculin tail domain; aa, amino acids; E15.5 and E18.5, embryonic day 15.5 and 18.5, respectively.

of PCR using the primers LacZ-GSP3 (5′-CCAGGGTTTTCCCAGTC-3′) and 5′RACE-AUAP (5′-GGCCACGCGTCGACTAGTAC-3′). The product of the second PCR was then cloned into the vector pT7-Blue (Novagen, Madison, WI) and sequenced using an automated sequencer (model 377A; PerkinElmer Life Sciences).

Assay for Proliferation—The cells were plated onto 96-well culture plates at a density of 1×10^3 cells/well (designated as day 0) and cultured in DMEM/F-12 medium supplemented with 5% FBS and ITS. Then the cell number in each well was evaluated by a 3-(4,5-dimethylthiazol-2-yl)-5-(3-carboxymethoxyphenyl)-2-(4-sulfophenyl)-2H-tetrazolium, inner salt assay performed using a CellTiter 96® Aqueous One solution cell proliferation assay kit (Promega, Madison, WI) according to the manufacturer's instructions. Proliferation of the cells was also assayed using a Calbiochem BrdU cell proliferation assay kit (Merck).

Reverse Transcription-Polymerase Chain Reaction (RT-PCR) and Real-time PCR—Total RNA (2.5 μg) treated with DNase (Qiagen) was reverse transcribed using random hexamer (Promega) and SuperScript II (Invitrogen). PCR was performed using *Taq* polymerase (Takara) and the specific primer sets summarized in supplemental Table S1. Amplification of the expected fragments was confirmed by sequencing of the products. For real-time PCR, we utilized TaqMan® gene expression assays with the 7300 real-time PCR system (Applied Biosystems). To generate a standard curve for real-time PCR, the amplicons of interest were first cloned into the pT7-Blue vector (Novagen), and serial 10-fold dilutions of the constructed plasmid were included in the assay. Samples were analyzed in triplicate. The copy number of the target cDNA in each sample was estimated by referring to the standard curve, which was standardized by that of *Gapdh* in each sample.

Plasmids and Recombinant Adenoviruses—The plasmid carrying a full-length cDNA for mouse vinculin (accession number AK077850) was obtained as the RIKEN® PHANTOM™ clone pFLC1-vinculin (clone ID 5930419L09). The fragment excised from pFLC1-vinculin by digestion with SfiI was inserted into pcDNA3.1-Zeo (Invitrogen), yielding pcDNA-vinculin(WT). We then constructed pcDNA-vinculin(WT)-V5 and pcDNA-vinculin(WT)-Myc encoding the carboxyl-terminal V5- and Myc-tagged forms of wild-type vinculin, respectively, by mutating the stop codon to introduce a new ClaI site using the QuikChange site-directed mutagenesis kit (Stratagene, La Jolla, CA), where annealed oligomers corresponding to the tags were inserted. The plasmid encoding the V5-tagged truncated mutant of vinculin (aa 1–624) was constructed by cloning of the corresponding fragment to pcDNA4.0/V5-His in frame (pcDNA4.0-vinculin(1–624)-V5).

To generate adenoviral vectors, the cDNAs corresponding to the wild-type vinculin and the mutant proteins were subcloned into pENTR11 (Invitrogen), and the inserts were transferred to the pAd/CMV/V5-DEST vector (Invitrogen). Recombinant adenoviruses were prepared with the ViraPower™ Adenovirus Expression System (Invitrogen). For comparison, we constructed vectors encoding the carboxyl region of vinculin corresponding to aa 625–1066 also, by removing the fragment for aa 2–624 from pENTR-vinculin(WT).

To construct the expression plasmid encoding paxillin, we first performed PCR-based cloning of cDNA for mouse paxillin using RNA derived from ATDC5 cells. Then the cDNA was cloned in frame into a pcDNA4/Myc-His vector (Invitrogen) after the stop codon was mutated to a EcoRI recognition site, resulting in a plasmid encoding paxillin fused to a Myc tag at the carboxyl terminus (designated pcDNA-paxillin-Myc-His).

Gene Silencing—Gene silencing in ATDC5 cells was performed using the siPORT Amine transfection agent (Applied Biosystems) and *Silencer*® Select siRNAs (Applied Biosystems) by the reversal transfection method. As the vinculin-specific siRNA, Silencer® Select siRNAs s75918 and s75919 were utilized. A negative control siRNA with a scrambled sequence was also included in the experiments.

The knocking down of vinculin expression in primary chondrocytes and the organ culture of metatarsals was performed by adenovirus-mediated expression of microRNA (miRNA) using the BLOCK-iT™ Pol II miR RNAi Expression Vector Kit with EmGFP and BLOCK-iT™ Pol II miR RNAi Select (Mmi526082 and Mmi526083) (Invitrogen).

Western Blotting—Whole cell extracts were harvested in radioimmune precipitation buffer (1% Triton, 1% sodium deoxycholate, 0.1% SDS, 150 mM NaCl, 10 mM Tris-Cl (pH 7.4), 5 mM EDTA, 1 mM orthovanadate and protease inhibitor mixture (Complete™, Roche Applied Science)). The cell lysates containing 10 μg of each protein were then subjected to SDS-PAGE and transferred to PVDF membranes (Bio-Rad). After blocking with BlockAce reagent (Dainippon Pharmaceuticals, Osaka, Japan) or Blocking-one reagent (Nacalai Tesque), the membranes were incubated with the following primary antibodies: polyclonal antibody against the amino or carboxyl terminus of vinculin (N-19 and C-20, respectively; Santa Cruz Biotechnology, Inc., Santa Cruz, CA), anti-β-galactosidase polyclonal antibody (Rockland, Gilbertsville, PA), anti-phospho-FAK antibody, anti-FAK antibody, anti-paxillin antibody (BD Transduction Laboratories, Franklin Lakes, NJ), anti-V5 antibody (Invitrogen), anti-cMyc antibody, anti-Sox9 antibody (Santa Cruz Biotechnology, Inc.), anti-phospho-Sox9 (Ser(P)-181) antibody (AnaSpec Inc., San Jose, CA), anti-phospho ERK1/2 antibody, anti-ERK1/2 antibody, anti-phospho-Akt antibody, anti-Akt antibody, anti-phospho-SHP2 (Src homology 2 domain-containing tyrosine phosphatase 2) antibody, anti-SHP2 antibody, anti-phospho-p38 MAPK antibody, anti-p38 MAPK antibody, anti-phospho-Smad antibodies, and anti-Smad antibodies (Cell Signaling, Beverly, MA). After incubation with the corresponding horseradish peroxidase (HRP)-conjugated secondary antibody, the proteins were visualized using the enhanced chemiluminescence (ECL) detection system (Amersham Biosciences).

Immunoprecipitation—Whole cell lysates were harvested in a lysis buffer (5 mM EDTA, 150 mM NaCl, 0.5% Nonidet P-40, 10% glycerol, and 10 mM Tris-HCl, pH 8.0) containing a protease inhibitor mixture (Complete™, EDTA-free, Roche Applied Science). The lysates were incubated with an antibody, and the immunocomplex was immobilized on protein A/G-agarose conjugate at 4 °C overnight. The agarose beads were extensively washed, and the immunoprecipitates were subjected to Western blot analyses.

Immunohistochemistry—Tibiae obtained from E18.5 mouse embryos or the cultured metatarsal bones were fixed in 10% buffered formalin and embedded in paraffin. Sections were deparaffinized, rehydrated, and subjected to antigen retrieval. The quenching of endogenous peroxidase activity and immunohistochemical staining were performed using ImmunoCruz staining systems (Santa Cruz Biotechnology, Inc.). After blocking, the sections were incubated with anti-vinculin antibody (Santa Cruz Biotechnology, Inc.), anti-Col II mouse monoclonal antibody (Clone 2B1.5; Thermo Fisher Scientific, Waltham, MA), or anti-aggrecan antibody (Santa Cruz Biotechnology, Inc.). Normal IgG was used as a negative control. Thereafter, the sections were incubated with biotinylated secondary antibodies and with HRP-conjugated streptavidin. Development of the peroxidase staining was done with 3′,3-diaminobenzidine. Antigen retrieval was performed by incubating the sections in 10 mM citrate buffer (pH 6.0) at 95 °C for 15 min, in pepsin solution (Thermo Fisher Scientific) at 37 °C for 60 min, or in 0.02% hyaluronidase (Sigma-Aldrich) in 0.1 M sodium acetate (pH 5.0) at 37 °C for 60 min, for staining with the anti-vinculin antibody, anti-Col II antibody, or anti-aggrecan antibody, respectively. The sections were counterstained with hematoxylin.

Cell Attachment Assay—Cells were trypsinized, and the reaction was neutralized with a trypsin inhibitor (Invitrogen). Then the cells suspended in serum-free medium (5×10^5 cells) were plated on fibronectin-coated dishes. After 30, 60, or 90 min of incubation, the non-attached cells were removed by washing, and the attached cells were harvested by trypsinization and counted.

Cell Migration Assay—To evaluate the ability of the cells to migrate, we performed a wound healing assay using culture inserts intended for this purpose (Ibidi GmbH, München, Germany), according to a previous report (18). Each insert has two wells with a 500-μm gap. The inserts were placed on culture plates, and cells were plated in both wells (7×10^3 cells/well, whose growth area was 2×0.22 cm^2). When the cells reached confluence, the medium was changed to serum-free medium. Ten hours later, the inserts were removed, and cells were incubated at 37 °C in a CO_2 incubator. The cells were subjected to microscopy to evaluate the narrowing of the cell-free gap.

Statistical Analysis—Data were analyzed using one-way analysis of variance. The method of Tukey was used for post hoc tests. All statistical analyses were conducted using Dr. SPSS II software.

RESULTS

Isolation of Clone in Which Gene Encoding Vinculin Was Trapped—Because the trap vector pPT1-geo possesses the *lacZ-neo* fusion gene *geo*, clones can be isolated on selection with neomycin only when the trapped gene is expressed in ATDC5 cells. We obtained 815 neomycin-resistant clones and subjected the clones with 10-fold more β-galactosidase activity than the parental cells to chondrogenic induction. We then further analyzed clone 4-17, which exhibited fewer mineralized nodules. The β-galactosidase activity in clone 4-17 was ~13-fold that in parental cells (Fig. 1*A*). The trap vector was inserted at only one location (Fig. 1*B*). A 5′-RACE analysis demonstrated that the vector was inserted into intron 13 of the vinculin gene (accession number NC_000080.5). The trapped allele was assumed to express a fusion protein containing the talin-binding head domain of vinculin and the product of *geo* but lacking the paxillin-binding tail domain of vinculin (Fig. 1*C*). Western blotting confirmed the production of the fusion protein (Fig. 1*D*). Interestingly, Western blotting using the antibody against the carboxyl terminus of vinculin, which was absent from the mutant protein, demonstrated comparable amounts of wild-type vinculin between the parental cells and clone 4-17 (Fig. 1*D*). Staining of clone 4-17 for β-galactosidase suggested the cytoplasmic distribution of the fusion product (data not shown). Clone 4-17 accumulated less cartilaginous matrix than the parental cells, as shown by Alizarin red and Alcian blue staining (Fig. 1, *E* and *F*). Staining with crystal violet verified the adhesion of the cells to the culture plates (Fig. 1, *E* and *F*). In contrast to clone 4-17, most of the other clones exhibited no obvious change in Alizarin red and Alcian blue staining (supplemental Fig. S1).

Expression of Vinculin Increased during Chondrocyte Differentiation—Immunostaining with the anti-vinculin antibody was performed using sections of tibiae harvested from E18.5 wild-type mouse embryos. Chondrocytes were positively stained, and the immunoreactivity was intense in hypertrophic chondrocytes (Fig. 2*B*).

We also examined the temporal expression pattern of vinculin in primary chondrocytes isolated from ribcages of wild-type newborns. The increasing expression of *Col10a1*, the gene for type X collagen and a marker for hypertrophic chondrocytes, indicated the progression of the differentiation during the culture (Fig. 2*D*). The expression of vinculin also was increased as the chondrocytes matured (Fig. 2, *C* and *E*).

To examine the temporal expression of vinculin in the parental ATDC5 cells and clone 4-17, these cells were cultured in the chondrogenic medium. The expression of *Sox9*, the key transcription factor for chondrocytic differentiation, reached a maximum at 4 weeks of culture in both cells. The expression of *Alp* (alkaline phosphatase) was lower in clone 4-17. To examine the expression of vinculin by RT-PCR, we used a pair of primers that amplified the fragment corresponding to the amino terminus of vinculin shared by the transcript from the wild-type allele and that from the trapped allele and found a temporal increase in both cells. In clone 4-17, the expression of *lacZ* was also elevated during the culture (Fig. 2*F*). To examine whether or not the trapping of vinculin altered the fate of the cells, we analyzed the expression of *MyoD1* and *Pparg*, markers for myocytes and adipocytes, respectively, and found no expression (data not shown).

Alteration in Signaling Induced by Adhesion to ECM in Clone with Trapped Vinculin Gene—The increase in the expression of vinculin during chondrocyte differentiation suggested some role in chondrogenesis. To investigate this role, we further characterized clone 4-17.

To characterize the truncated vinculin derived from the trapped allele, we constructed plasmids encoding a V5-tagged wild-type vinculin (pcDNA-vinculin(WT)-V5) or a truncated protein corresponding to the mutant derived from the trapped allele (pcDNA-vinculin(1–624)-V5). For comparison, we constructed another plasmid encoding the carboxyl fragment of

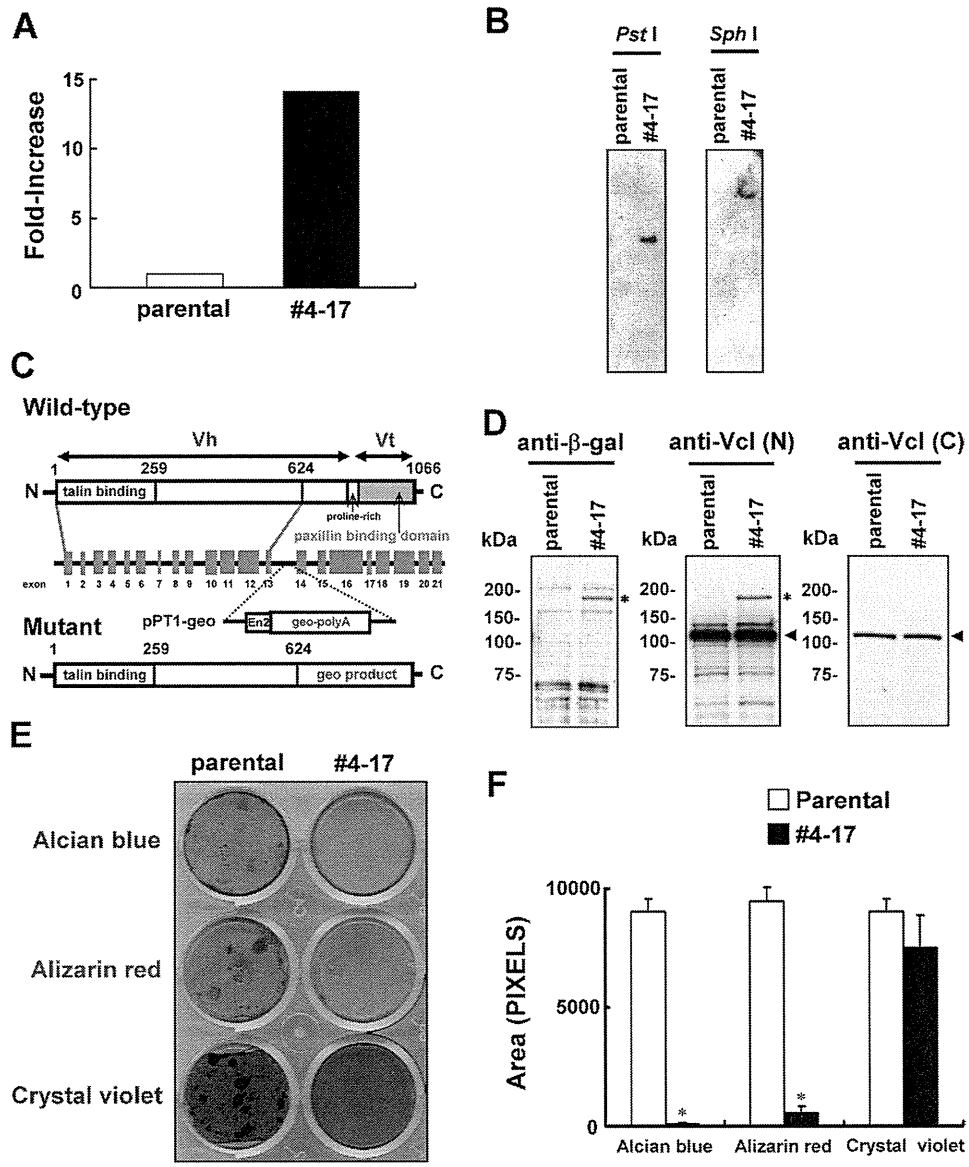

FIGURE 1. **Isolation of the clone with the trapped vinculin gene.** *A*, the β-galactosidase activity in clone 4-17 and the parental ATDC5 cells. *B*, Southern blotting. Genomic DNA was digested with the restriction enzyme PstI or SphI, and subjected to hybridization with a radiolabeled fragment of *lacZ* cDNA prepared by EcoRI/SacI digestion of pPT1-geo. *C*, genomic organization of the murine vinculin gene and the insertional mutation resulting from the gene trapping. The locations of exons (*gray boxes*) and introns (*horizontal lines between exons*) are indicated. pPT1-geo was inserted into intron 13, resulting in a mutant protein in which vinculin lacking the tail domain was fused to the *geo* product. *D*, detection of the β-galactosidase fusion protein. Cell lysates were subjected to immunoblotting using antibodies against β-galactosidase (*left*) or amino-terminal (*center*) or carboxyl-terminal vinculin. The *asterisk* and the *arrow* indicate the signals corresponding to the fusion protein comprising part of vinculin and the *geo* product and that for wild-type vinculin, respectively. *E*, impaired chondrogenic nodule formation in clone 4-17. The cells were cultured for 8 weeks in chondrogenic medium and subjected to Alcian blue and Alizarin red staining. Clone 4-17 accumulated less cartilaginous matrix than parental cells. The cells were also stained with crystal violet to confirm the adhesion to culture plates. *F*, the stained area in *E* was quantitated using NIH Image 1.63 software. Data are shown as the mean ± S.D. (*error bars*) ($n = 3$). *, $p < 0.001$ *versus* parental cells.

vinculin (pcDNA-vinculin(625–1066)-V5), which lacked the region retained in the trapped allele, also. Co-immunoprecipitation experiments confirmed that the truncated vinculin(1–624) exhibited impaired binding to paxillin (Fig. 3*A*). The binding to talin was markedly increased in the truncated vinculin(1–624) compared with in vinculin(WT) (Fig. 3*B*).

Mouse embryo fibroblasts isolated from vinculin-knock-out mouse embryos demonstrated increased phosphorylation of focal adhesion kinase (FAK) and extracellular signal-regulated kinase (ERK) in response to adhesion to ECMs (12). Therefore, we examined the phosphorylation of FAK at Tyr-397 and ERK1/2 induced by adhesion to ECMs in clone 4-17 and the parental ATDC5 cells. The phosphorylation of FAK and ERK1/2 induced by adhesion to both fibronectin (FN) and type II collagen (Col II) was increased in clone 4-17 (Fig. 3, *C–E*). The knockdown of vinculin expression in parental cells also resulted in an increase in the adhesion-induced phosphorylation of FAK and ERK1/2 (Fig. 3*F*). Because transfection of siRNA may have toxic effects, we confirmed that the expression of vinculin was completely reversed at 9 days after the transfection of gene-specific siRNA (supplemental Fig. S2). The data indicate that

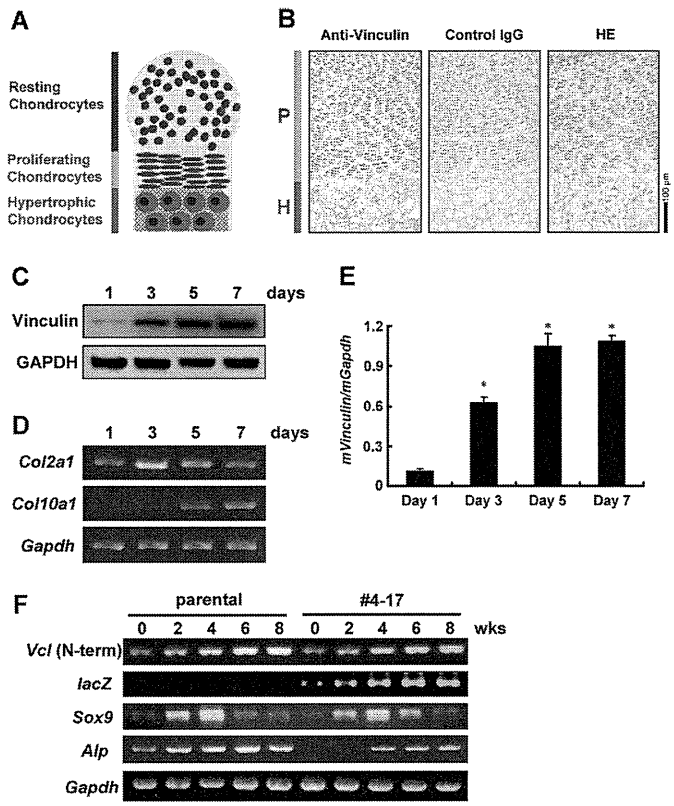

FIGURE 2. **Increasing expression of vinculin during the differentiation of chondrocytes.** *A*, illustration of endochondral bone formation displayed as a layered structure. *B*, immunostaining of mouse tibiae from an E18.5 embryo with anti-vinculin antibody. The immunoreactivity was intense in hypertrophic chondrocytes. *P* and *H*, proliferating and hypertrophic chondrocytes, respectively. *HE*, hematoxylin/eosin-stained section. *C–E*, increasing expression of vinculin during the maturation of primary chondrocytes. Chondrocytes isolated from mouse ribcages were cultured for the period indicated before being harvested for Western blotting (*C*) and real-time PCR (*E*). In *E*, data are shown as the mean ± S.D. (*error bars*). *, $p < 0.05$ *versus* day 1. The temporal expression of *Col2a1* and *Col10a1* analyzed by RT-PCR is shown in *D*. *F*, RT-PCR analyses for the temporal expression of the amino-terminal fragment of vinculin, *Sox9*, and *Alp* (alkaline phosphatase) during the chondrocytic differentiation of parental ATDC5 cells and clone 4-17. The primer set for amino-terminal vinculin amplifies the fragment derived from both the wild-type and trapped alleles.

vinculin functions as a negative regulator of the signaling induced by adhesion to ECM. Considering the similarity in the increase in the adhesion-induced phosphorylation of FAK and ERK1/2 between the vinculin-silenced cells and clone 4-17, we assume that the truncated vinculin derived from the trapped allele has some dominant effect that interferes with the functions of wild-type vinculin. Consistent with this notion, exogenous expression of vinculin(1–624)-V5 into the parental cells also increased the adhesion-induced phosphorylation of FAK, and the simultaneous overexpression of wild-type vinculin failed to abolish the increase (Fig. 3*G*). On the other hand, exogenous expression of the carboxyl fragment vinculin(625–1066)-V5 into the parental cells had no obvious influence on the adhesion-induced phosphorylation of FAK (Fig. 3*H*).

To elucidate the mechanism by which the truncated vinculin(1–624)-V5 exerted a dominant negative effect on signaling, we examined whether the mutant affected the interaction between the wild-type vinculin and talin. COS7 cells were transfected with Myc-tagged wild-type vinculin (vinculin(WT)-Myc) together with vinculin(WT)-V5 or the mutant vinculin(1–624)-V5, and the lysates were subjected to immunoprecipitation using anti-talin antibody. Aliquots of the immunoprecipitates were subjected to immunoblotting with anti-Myc antibody, and the proteins were visualized using ECL Plus™ reagent (Amersham Biosciences) with high sensitivity. The co-transfection of vinculin(1–624)-V5 reduced the co-immunoprecipitation of vinculin(WT)-Myc with talin (Fig. 3*I*). These results suggest that vinculin(1–624) interferes with the interaction between the wild-type vinculin and talin, which might be the mechanism for the dominant negative effect of the mutant.

Effects of Trapping of Vinculin Gene on Cell Proliferation, Attachment, and Migration in Vitro—We next examined the effects of the trapping of the vinculin gene on cell behavior *in vitro*. The proliferation was comparable between the parental cells and the clone 4-17 with the trapped vinculin gene (Fig. 4, *A* and *B*). As for the attachment to the ECM and motility, there was no obvious difference between the parental cells and clone 4-17 (Fig. 4, *C* and *E*) either, which was probably due to the activity of the remaining wild-type allele in clone 4-17. We also examined the effects of the knockdown of vinculin in parental cells, which slightly reduced the attachment and increased the cell migration (Fig. 4, *D* and *F*). Trapping of the vinculin gene in clone 4-17 had no apparent effect on focal adhesion. Knockdown of vinculin in parental cells had no obvious influence on focal adhesion either. These observations suggest the residual activity of vinculin to be enough for focal adhesion *in vitro* (Fig. 4*G*).

Defects in Chondrocytic Differentiation in Clone with Trapped Vinculin Gene—To clarify whether vinculin plays a role in chondrogenesis, we further analyzed the chondrocytic phenotype of clone 4-17. Parental ATDC5 cells and clone 4-17 were cultured in the chondrogenic medium, and the temporal expression of the chondrocytic marker genes was evaluated (Fig. 5). The expression of *Sox9* was retained in clone 4-17. However, the expression of *Col2a1* encoding the a1 chain of Col II as well as that of aggrecan was markedly reduced in clone 4-17. Sox5 and Sox6 are transcription factors that cooperate with Sox9 in chondrocytic differentiation. Although the expression of *Sox5* was retained in clone 4-17, that of *Sox6* was decreased (Fig. 5). The expression of *Ihh*, a marker for prehypertrophic chondrocytes, peaked at 6 weeks of culture in the parental cells. In clone 4-17, it reached a maximum at 4 weeks of culture and declined thereafter. The expression of *Ihh* in clone 4-17 suggested that at least some cells differentiated into prehypertrophic chondrocytes. The expression of *Col10a1* gradually elevated during the differentiation of parental ATDC5 cells, whereas it markedly decreased in clone 4-17. Runx2 is a transcription factor that plays a critical role in chondrocyte maturation and directly controls *Col10a1* expression (19). The expression of *Runx2* increased during the later differentiation in the parental cells but not in clone 4-17 (Fig. 5).

Knockdown of Vinculin or Expression of Mutant Vinculin(1–624) Caused Impaired Maturation in Primary Chondrocytes—We also examined the effects of knocking down the expression of vinculin expression using primary chondrocytes. Primary chondrocytes were plated on day 0 and, 24 h later, infected with an adenovirus encoding vinculin-specific miRNA or control miRNA.

Alcian blue staining demonstrated less accumulation of cartilaginous matrix in the cells where the expression of vinculin was knocked down, a situation that was rescued by the simultaneous introduction of the adenovirus encoding wild-type vinculin (Fig. 6, *A* and *B*). The expression of neither *Sox9* nor *Sox5* was influenced, whereas that of *Sox6* on day 7 was suppressed by knocking down the expression of vinculin. The expression of *Col2a1* and aggrecan on day 3 was also markedly decreased, and that of *Ihh* was reduced on both day 3 and day 7 by the knockdown. As for the expression of *Col10a1*, which was detected on day 7 in the control cells, the knockdown of vinculin resulted in its reduction. The expression of *Runx2* also was decreased by the knockdown (Fig. 6*E*). These alterations in gene expression were consistent with those in clone 4-17. Adenoviral transfer of the truncated vinculin(1–624)-V5 in primary chondrocytes also resulted in the reduced expression of *Col2a1*, aggrecan, *Sox6*, *Ihh*, *Col10a1*, and *Runx2* and less accumulation of cartilaginous matrix (Fig. 6*F* and supplemental Fig. S3). On the other hand, adenoviral transfer of the carboxyl fragment vinculin(625–1066)-V5 in primary chondrocytes had no obvious influence on the accumulation of cartilaginous matrix (data not shown).

Knockdown of Wild-type Vinculin as Well as Expression of Vinculin(1–624) Impaired Growth of Metatarsal Explants— The role of vinculin in chondrogenesis was further investigated using organ cultures of metatarsal rudiments *ex vivo*. Metatarsals from E15.5 mouse embryos were infected with an adenovirus for vinculin-specific miRNA or control miRNA and cultured for 7 days. In this system, the rudiments grew during the culture. In the sections cut from the rudiments, the direct fluorescence of EmGFP derived from the vectors encoding miRNAs was detected

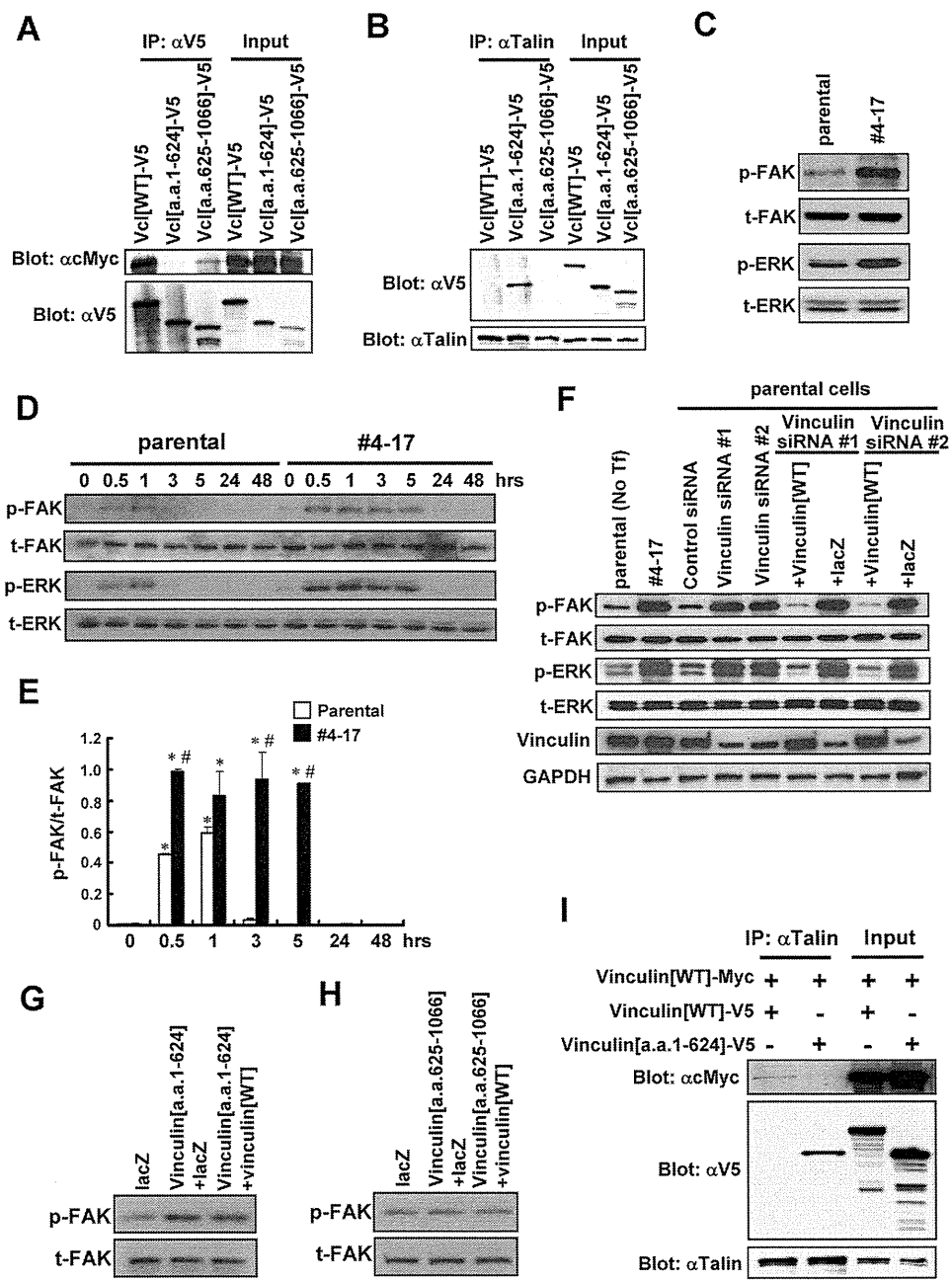

in chondrocytes as well as in the perichondrium, demonstrating the infection in these cells (supplemental Fig. S4). We found that the extended length was shorter in the rudiments infected with vinculin-specific miRNA. Moreover, simultaneous infection with the virus encoding wild-type vinculin, but not the control virus encoding *lacZ*, restored the blunted growth due to the knockdown of vinculin (Fig. 7, *A* and *B*). Hematoxylin/eosin (H&E) staining of sections cut from the rudiments demonstrated that the columnar proliferation of the chondrocytes was disturbed, and the subsequent hypertrophic change was insufficient in the rudiments with the knockdown of vinculin (Fig. 7, *C* and *D*). In immunohistochemistry, immunoreactivity with the antibodies against Col II and aggrecan was decreased in the rudiments infected with vinculin-specific miRNA (Fig. 7, *E* and *F*). Real-time PCR analyses using RNA extracted from the rudiments demonstrated that the knockdown of vinculin caused the reduced expression of *Col2a1* and aggrecan. The expression of *Runx2* also was decreased by the knockdown of vinculin, whereas that of *Sox9* was retained (Fig. 7*G*). Adenoviral transfer of the truncated vinculin(1–624)-V5 also impaired the growth of the metatarsal rudiments (supplemental Fig. S5).

Altered Signaling during Chondrocytic Differentiation in Cells with Knocked Down or Trapped Vinculin Gene—Thus, vinculin appears to play an important role in chondrogenesis. Therefore, we next investigated the mechanism by which vinculin regulates chondrocyte differentiation.

Several signaling pathways have been implicated in chondrogenesis. The phosphorylation of ERK1/2, SHP2, and Akt as well as that of FAK increased during the maturation of primary chondrocytes. In addition, the phosphorylation of p38 MAPK and some Smads also increased as the chondrocytes matured (Fig. 8*A*). Therefore, we examined whether the impaired functioning of vinculin affected the phosphorylation of these signaling molecules. Knockdown of vinculin in primary chondrocytes resulted in the decreased phosphorylation of ERK1/2 on both day 3 and day 7 of culture and reduced phosphorylation of FAK on day 7. On the other hand, the phosphorylation of SHP2 on day 3 and day 7 as well as that of Akt on day 3 increased with the knockdown of vinculin expression (Fig. 8, *B* and *C*). We also analyzed the phosphorylation of these proteins during the differentiation of parental ATDC5 cells and clone 4-17 with the trapped vinculin gene and obtained consistent results. Phosphorylation of FAK and ERK1/2 was decreased in clone 4-17 as compared with in parental cells after 2 weeks of culture. On the other hand, phosphorylation of SHP2 and Akt was stronger in clone 4-17 than in parental cells during weeks 0–4 (Fig. 8, *D* and *E*).

Interestingly, we found that the phosphorylation of p38 MAPK was markedly reduced in chondrocytes with vinculin knocked down as well as in clone 4-17, suggesting that dysfunctional vinculin impaired the activation of the p38 MAPK pathway in differentiating chondrocytes. We also examined the phosphorylation of some Smads, which was not affected by the dysfunctional vinculin (Fig. 8, *B–E*).

The reduced phosphorylation of FAK and ERK1/2 during the chondrocytic differentiation shown in Fig. 8 makes a striking contrast to the increase in adhesion-induced phosphorylation of FAK and ERK1/2 in the cells in which vinculin was knocked down or trapped (Fig. 3). Therefore, we performed another series of experiments to examine the phosphorylation of FAK, ERK1/2, and SHP2 at 0, 5, 10, 24, 48, 72, and 120 h after the cells were plated (supplemental Fig. S6). At the time points of 0–48 h, the phosphorylation of FAK and ERK was increased in the clone 4-17 compared with in parental cells, which was consistent with the results shown in Fig. 3, where the phosphorylation was examined 0.5–5 h after the cells were plated. On the other hand, at the time points of 72 and 120 h, FAK and ERK phosphorylation was stronger in the parental cells than in clone 4-17, which was consistent with the results in Fig. 8, where the phosphorylation was examined at 0–8 weeks. Thus, these results demonstrate that the phosphorylation of FAK and ERK was initially increased and then suppressed in the cells with a trapped vinculin gene compared with the parental cells after they adhered. The phosphorylation of SHP2 was increased in clone 4-17 at 72 and 120 h, which might be involved in the reduced phosphorylation of ERK and FAK (supplemental Fig. S6).

FIGURE 3. **Alteration in the signaling induced by adhesion to ECM in the clone 4-17 and the cells with the vinculin gene knocked down.** *A*, the truncated vinculin derived from the trapped allele was unable to bind to paxillin. COS7 cells were transfected with the expression plasmid encoding Myc-tagged paxillin (*paxillin-Myc*) together with the plasmid encoding V5-tagged wild type (*vinculin(WT)-V5*), the truncated vinculin corresponding to the mutant derived from the trapped allele in clone 4-17 (*vinculin(1–624)-V5*), or the mutant encoding the carboxyl fragment of vinculin (*vinculin(625–1066)-V5*), and lysates were harvested for immunoprecipitation (*IP*) using anti-V5 antibody. The immunoprecipitates and the input protein (10 μg) were subjected to Western blotting using the indicated antibodies. *B*, the binding to talin was enhanced in the truncated vinculin derived from the trapped allele. COS7 cells were transfected with the plasmid encoding vinculin(WT)-V5, vinculin(1–624)-V5, or vinculin(625–1066)-V5, and lysates were used for immunoprecipitation with anti-talin antibody. The immunoprecipitates and the input protein (10 μg) were subjected to Western blotting with the indicated antibodies. *C*, increase in phosphorylation of FAK at Tyr-397 and ERK1/2 induced by adhesion to FN in clone 4-17. Parental ATDC5 cells or clone 4-17 were plated onto FN. Thirty minutes later, lysates were harvested for Western blot analyses. *D* and *E*, increase in phosphorylation of FAK at Tyr-397 and ERK1/2 induced by adhesion to Col II in clone 4-17. Cells were plated onto Col II, and lysates were harvested at the indicated time points. The densitometric ratio of the intensity of the signal corresponding to phosphorylated FAK to that of total FAK is shown in *E*. The data are shown as the mean ± S.D. (*error bars*) ($n = 3$). *, $p < 0.05$ *versus* 0 h; #, $p < 0.05$ *versus* parental cells. *F*, knockdown of vinculin in parental ATDC5 cells increased the adhesion-induced phosphorylation of FAK and ERK1/2, which was cancelled by simultaneous introduction of the expression plasmid encoding vinculin(WT). Lysates were harvested for Western blotting from the parental ATDC5 cells transfected with control siRNA, vinculin-specific siRNA with or without the expression plasmids encoding vinculin(WT) or *lacZ*, the non-transfection control, and clone 4-17 with the vinculin gene trapped 30 min after the plating onto FN. *G*, exogenous expression of the truncated vinculin(1–624) in parental ATDC5 cells increased the adhesion-induced phosphorylation of FAK, which was not abrogated by the simultaneous expression of exogenous wild-type vinculin. Lysates were harvested from the parental ATDC5 cells infected with the adenoviral vector for vinculin(1–624)-V5 together with that for *lacZ* or vinculin(WT)-V5 and the cells expressing *lacZ* alone 30 min after the plating onto FN. *H*, exogenous expression of the truncated vinculin(625–1066) in parental ATDC5 cells had no effects on the adhesion-induced phosphorylation of FAK. ATDC5 cells were infected with the vector for vinculin(625–1066)-V5 together with that for *lacZ* or vinculin(WT)-V5 and the cells expressing *lacZ* alone, and lysates were harvested 30 min after the plating onto FN. *I*, the truncated vinculin(1–624) interfered with the interaction between the wild-type vinculin and talin. COS7 cells were transfected with Myc-tagged wild-type vinculin (*vinculin(WT)-Myc*) together with vinculin(WT)-V5 or the mutant vinculin(1–624)-V5, and the lysates were subjected to immunoprecipitation using anti-talin antibody. The immunoprecipitates and the input protein (10 μg) were subjected to Western blotting using the indicated antibodies. In the immunoblot using anti-Myc antibody, the co-transfection of vinculin(1–624)-V5 reduced the signal for the co-immunoprecipitation of vinculin(WT)-Myc with talin. *p-FAK*, phosphorylated FAK; *t-FAK*, total FAK.

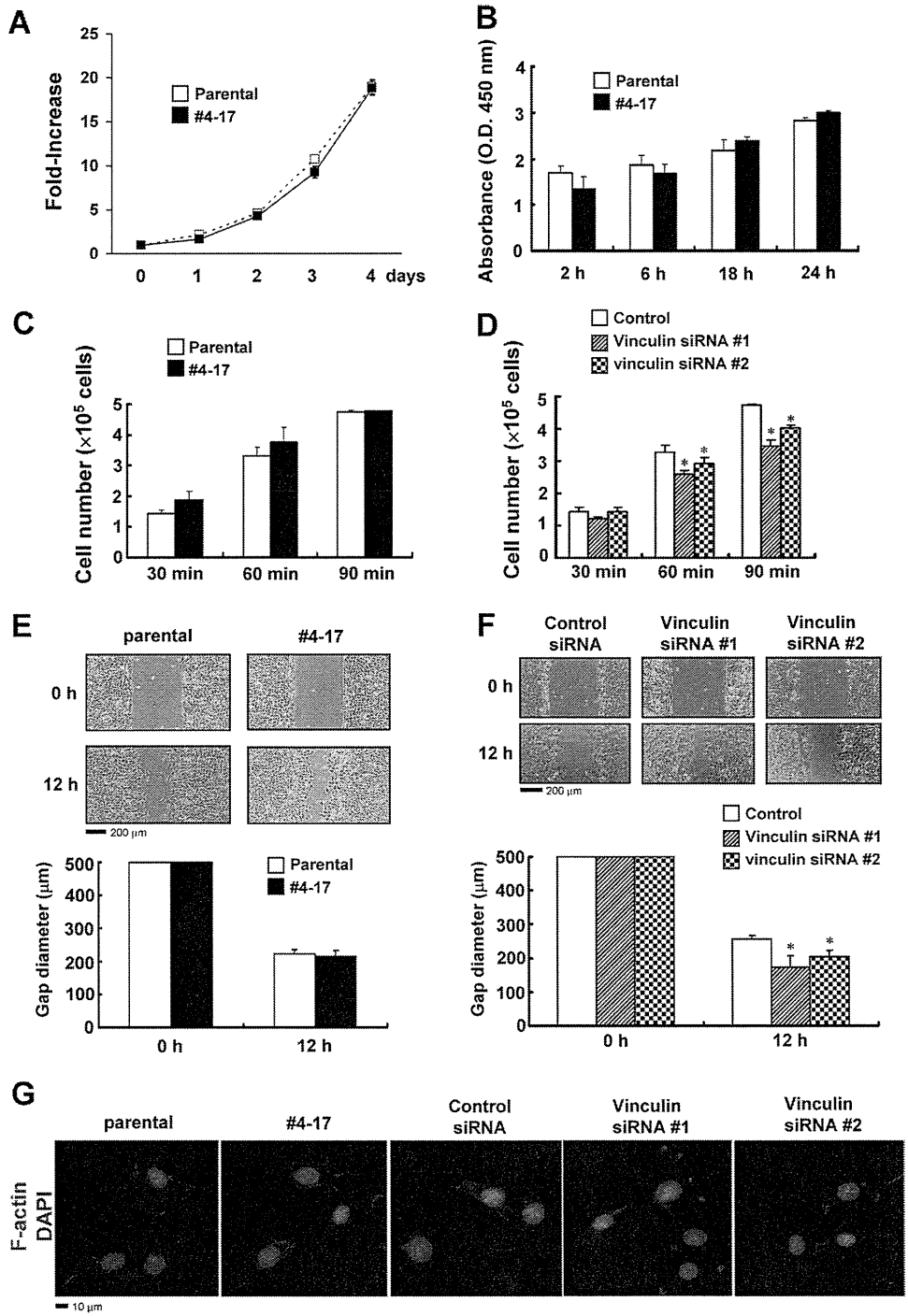

FIGURE 4. **Effects of the trapping or knockdown of the vinculin gene on the increase in cell number, attachment and migration.** *A* and *B*, no obvious difference in cell proliferation between parental ATDC5 cells and clone 4-17 with the trapped vinculin gene. In *A*, cells were plated in 96-well culture plates at a density of 1×10^3 cells/well (designated day 0) and cultured for the period indicated. The cell number in each well was evaluated by a 3-(4,5-dimethylthiazol-2-yl)-5-(3-carboxymethoxyphenyl)-2-(4-sulfophenyl)-2H-tetrazolium, inner salt assay, and the -fold increase from the value on day 0 was calculated. The data are shown as the mean ± S.D. (*error bars*) ($n = 4$). In *B*, a BrdU cell proliferation assay was performed. *C*, trapping of the vinculin gene had no obvious effect on cell attachment. The parental ATDC5 cells and clone 4-17 were plated onto FN-coated dishes, and the attached cells were counted after the period indicated. The data are shown as the mean ± S.D. ($n = 3$). *D*, attachment assay in the ATDC5 cells transfected with control siRNA or vinculin-specific siRNA. Cells were plated onto FN-coated dishes, and the attached cells were counted after the indicated period. The data are shown as the mean ± S.D. ($n = 3$). *, $p < 0.05$ *versus* control siRNA. *E*, trapping of the vinculin gene had no obvious effect on cell migration. Microscopic images of the parental ATDC5 cells and clone 4-17 assayed for their ability to close a defined 500-μm gap in a cell migration assay. We used defined culture inserts, the removal of which generated a 500-μm gap between cells. The gap diameters are shown as the mean ± S.D. ($n = 3$). *F*, a cell migration assay was performed in the parental ATDC5 cells transfected with control siRNA or vinculin-specific siRNA. The gap diameters are shown as the mean ± S.D. ($n = 3$). *, $p < 0.05$ *versus* control siRNA. *G*, trapping or knockdown of the vinculin gene resulted in no obvious change in focal adhesion. Parental ATDC5 cells, clone 4-17, and the cells transfected with vinculin-specific siRNAs or control siRNA were plated onto FN-coated coverslips and, 5 h later, fixed and stained with Alexa Fluor™ 555 phalloidin to examine the subcellular distribution of F-actin. Nuclei were stained with 4′,6-diamidino-2-phenylindole (*DAPI*).

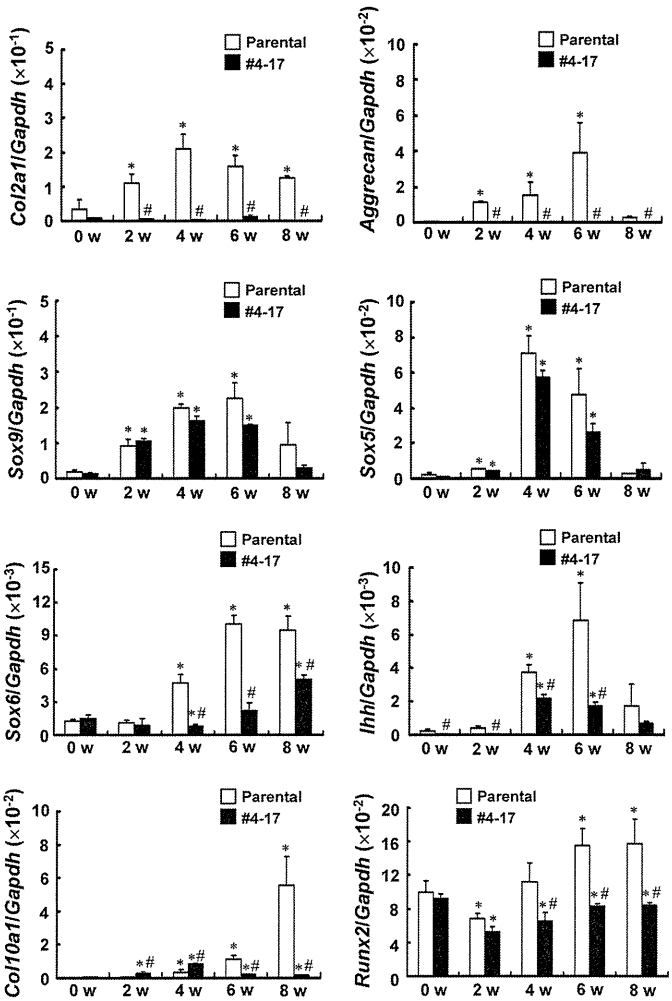

FIGURE 5. **Altered gene expression in clone 4-17 with the trapped vinculin gene.** Parental ATDC5 cells and clone 4-17 were cultured in the chondrogenic medium for the period indicated, before RNA was extracted for real-time PCR analyses. The copy number of the target cDNA in each sample was estimated by referring to a standard curve, which was standardized by that of *Gapdh*. The data are shown as the mean ± S.D. (*error bars*) ($n = 3$). *, $p < 0.05$ *versus* 0 weeks; #, $p < 0.05$ *versus* parental cells; *w*, weeks.

As shown in Fig. 5 and 6, trapping or knockdown of vinculin did not alter the mRNA expression of *Sox9*. Therefore, we examined whether the impaired functioning of vinculin affected the phosphorylation of the Sox9 protein. Neither trapping nor knockdown of the vinculin gene affected the phosphorylation of Sox9, suggesting that the function of Sox9 was retained in the cells with a dysfunctional vinculin (Fig. 8, *B* and *D*).

Impaired Functioning of Vinculin Blunted Responsiveness of Chondrocytes to IGF-I—Changes in the phosphorylation of signaling molecules during chondrocytic differentiation suggested that the knockdown or trapping of vinculin has an influence not only on signaling from the ECM but also on other signaling pathways, including those of growth factors. IGF-I exerts its signals via PI3K/Akt and MEK/ERK pathways. In addition, IGF-I is known to regulate *Col2a1* and aggrecan expression, both of which were down-regulated in the cells in which vinculin was trapped or knocked down. Therefore, we examined whether responsiveness to IGF-I was altered by the dysfunctional vinculin using the organ culture of metatarsal rudiments. The knockdown of vinculin expression impaired the IGF-I-induced growth in the rudiments (Fig. 9, *A* and *B*). Real-time PCR analyses revealed that treatment with IGF-I increased the expression of *Col2a1*, aggrecan, and a cell cycle-related gene, cyclin D1, in the control rudiments but not in those with the vinculin gene knocked down (Fig. 9*C*), suggesting that the dysfunctional vinculin blunted the responsiveness to IGF-I. The expression of IGF-I receptor was not altered by the knockdown of vinculin (data not shown).

DISCUSSION

The ECM provides a cell type-specific microenvironment and is recognized and bound by integrins and cell surface transmembrane receptors. Vinculin is a major component of the focal adhesion complex that acts as a mechano-coupler and an actin-binding protein. Several functions, mostly related to cell adhesion and motility processes, have been ascribed to vinculin. Cells depleted of vinculin show reduced adhesion to various ECM proteins and increased migration rates compared with wild-type cells (12–14). Despite profound roles in cell adhesion and motility, little is known about the tissue-specific functions of vinculin.

Because vinculin-knock-out mice die in the embryonic stage before skeletogenesis is initiated (12), the roles of vinculin in skeletal development have remained unclear. Results shown here clearly indicate that vinculin plays a critical role in chondrogenesis. Impaired functioning of vinculin in chondrocytes caused the decreased expression of *Col2a1* and aggrecan, which are markers for early chondrocytes (Figs. 5 and 6, *E* and *F*). It was interesting that the expression of *Sox9* was retained both in the vinculin-trapped clone and in cells with vinculin knocked down because Sox9 is a central transcription factor in chondrogenesis and regulates the expression of several chondrocyte-specific genes, including *Col2a1* and aggrecan (20, 21). Although the expression of *Sox6* was decreased in the cells with vinculin trapped or knocked down, this was unlikely to be the main cause for the reduced expression of *Col2a1* and aggrecan, because *Sox6* expression was detected after that of *Col2a1* and aggrecan in primary chondrocytes (Fig. 6*E*). In addition, Sox5 and Sox6 are functionally redundant, and the skeletal phenotype of *Sox6*-knock-out mice is mild (22). Our results suggest the complexity of the regulation of *Col2a1* and aggrecan expression.

In addition to the markers for early chondrocytes, the expression of those for later stages, such as *Col10a1* and *Runx2*, was also markedly reduced by a dysfunctional vinculin, and the mineralization was impaired. Because Runx2 is known to directly control the expression of *Col10a1* in hypertrophic chondrocytes, the reduced expression of *Runx2* is likely to be a cause for the decreased level of *Col10a1*. The activity of the Runx2 protein also might be impaired, because the suppression of *Col10a1* was so remarkable.

The impaired differentiation of chondrocytes with a dysfunctional vinculin indicates the critical roles of the signaling from the ECM in chondrogenesis. The importance of the signaling from the ECM in chondrogenesis was also suggested by

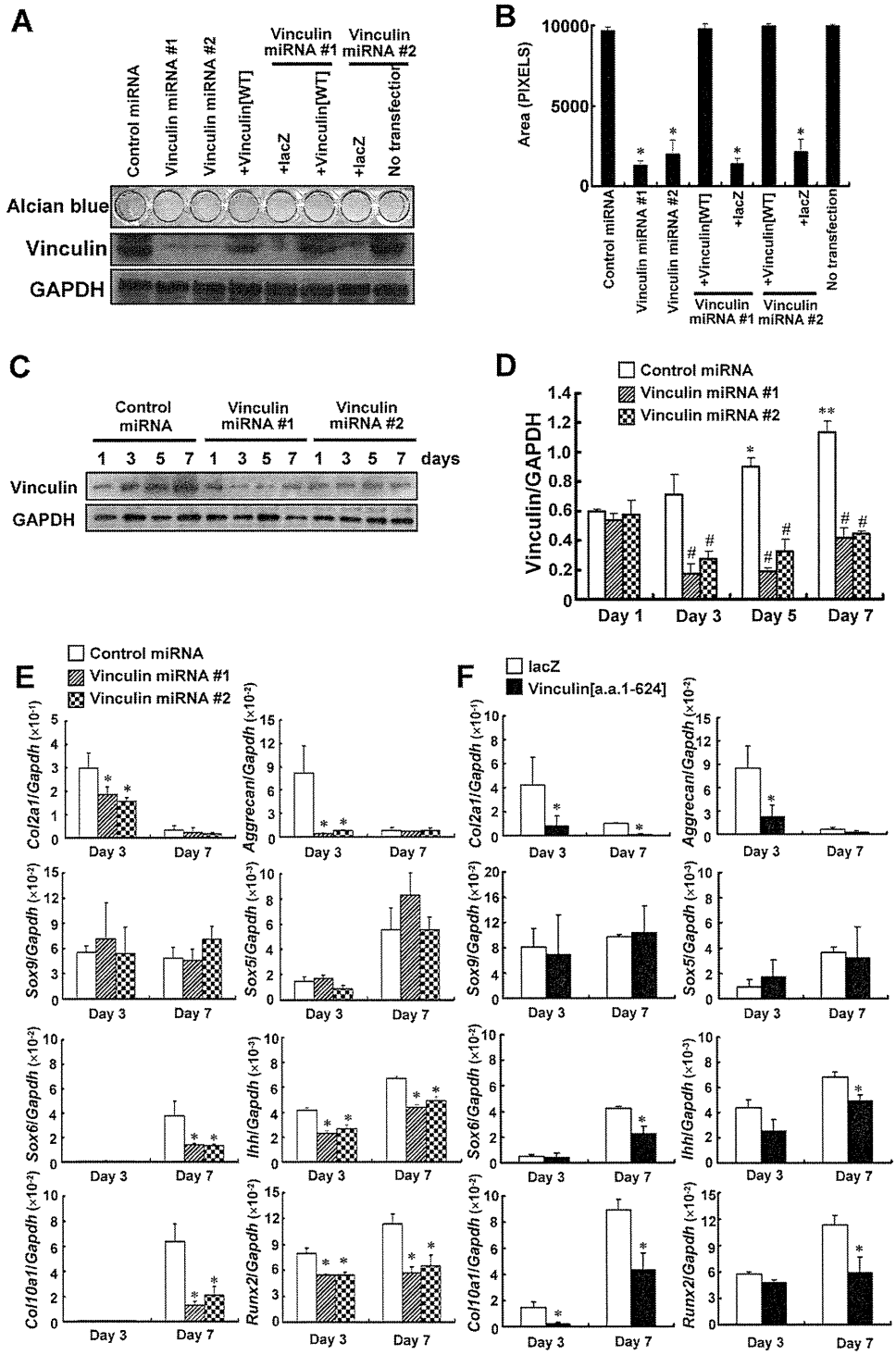

FIGURE 6. **Impaired maturation of the primary chondrocytes with the vinculin gene knocked down or the exogenous expression of the truncated mutant vinculin(1–624).** *A*, knockdown of vinculin expression in primary chondrocytes reduced the accumulation of cartilaginous matrices, which was rescued by simultaneous transfer of the adenovirus encoding vinculin(WT). Primary chondrocytes were plated onto 48-well culture plates (2×10^4 cells/well). The next day (day 1), the cells were infected with adenovirus encoding control miRNA or vinculin-specific miRNA with or without the virus for vinculin(WT)-V5 or *lacZ*. On day 7, the cells were subjected to Alcian blue staining or Western blotting. *B*, the Alcian blue-stained area in *A* was quantitated. The data are shown as the mean ± S.D. (*error bars*) ($n = 3$). *, $p < 0.05$ *versus* control miRNA. *C* and *D*, efficient knockdown of vinculin expression by gene-specific miRNA in primary chondrocytes. Cells were infected with an adenovirus encoding vinculin-specific miRNA or control miRNA on day 1, and lysates were harvested for Western blotting at the indicated time points. The densitometric ratio of the intensity of the signals corresponding to vinculin and to GAPDH is shown in *D*. The data are shown as the mean ± S.D. ($n = 3$). *, $p < 0.05$; **, $p < 0.01$ *versus* day 1; #, $p < 0.05$ *versus* control miRNA. *E*, the knockdown of vinculin expression in primary chondrocytes reduced the expression of *Col2a1*, aggrecan, *Sox6*, *Ihh*, *Runx2*, and *Col10a1*. Cells were infected with the adenovirus encoding vinculin-specific miRNA or control miRNA on day 1. RNA was extracted for real-time PCR on day 3 and day 7. The data are shown as the mean ± S.D. ($n = 3$). *, $p < 0.05$ *versus* control miRNA. *F*, expression of the truncated vinculin(1–624) in primary chondrocytes also reduced the expression of *Col2a1*, aggrecan, *Sox6*, *Ihh*, *Runx2*, and *Col10a1*. The data are shown as the mean ± S.D. ($n = 3$). *, $p < 0.05$ *versus lacZ*.

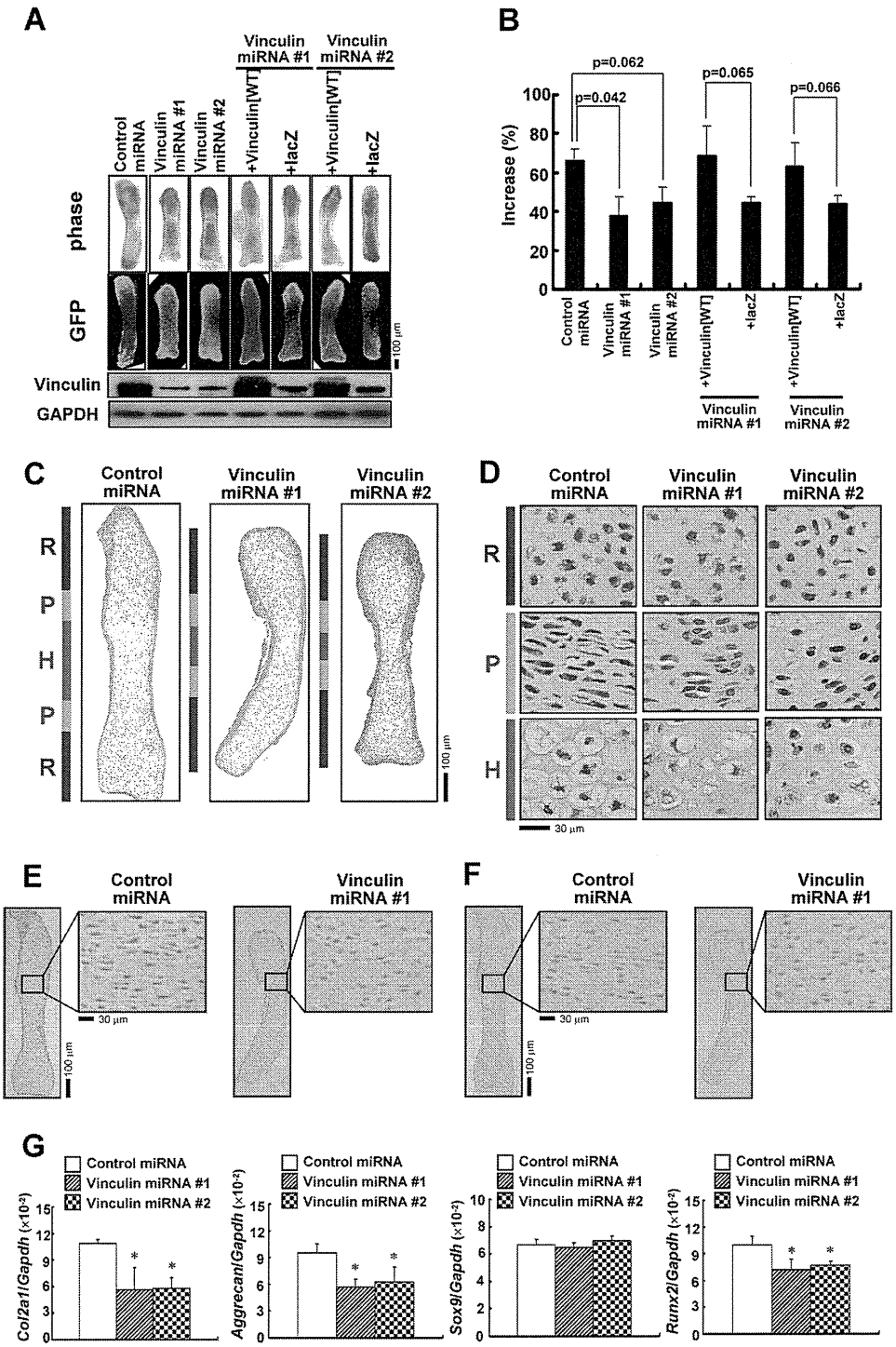

FIGURE 7. **Knockdown of vinculin expression in metatarsal organ cultures resulted in impaired linear growth.** *A* and *B*, knockdown of vinculin inhibited the linear growth of metatarsal rudiments. Metatarsals from E15.5 mouse embryos were infected with the adenovirus encoding control miRNA or vinculin-specific miRNA with or without the adenovirus for vinculin(WT) or *lacZ* after the measurement of initial length using a microscope and Image-Pro PLUS 6.3 software. On day 7, the length of the rudiments was measured again, and the protein was extracted for Western blotting. In *A*, representative images of the phase-contrast view and the direct fluorescence of EmGFP derived from the vector encoding miRNAs are depicted, together with the results of Western blotting using the indicated antibodies. In *B*, the increase in the length of the rudiments is shown as a percentage of the extended length during the culture to the initial length of each bone. The data are shown as the mean ± S.D. (*error bars*) ($n = 3$). *C* and *D*, HE-stained sections of metatarsal rudiments infected with adenovirus encoding control miRNA or vinculin-specific miRNA. *R*, *P*, and *H*, resting, proliferating, and hypertrophic zones, respectively. Higher power images are shown in *D*. *E* and *F*, immunostaining demonstrated the reduced expression of Col II (*E*) and aggrecan (*F*) in the metatarsal explants where the expression of vinculin was knocked down. *G*, real-time PCR for the genes indicated using RNA extracted from the metatarsal explants infected with vinculin-specific miRNA or control miRNA. Knockdown of vinculin suppressed the expression of *Col2a1*, aggrecan, and *Runx2* in the metatarsals.

the chondrodysplasia-like phenotype of chondrocyte-specific β1 integrin-knock-out mice and integrin-linked kinase-knock-out mice (23, 24). However, reduced proliferation of the chondrocytes was the main cause for the skeletal phenotype in these mice, and the expression of chondrocyte-specific genes, such as *Col2a1*, was comparable with that in wild-type mice. Thus, the

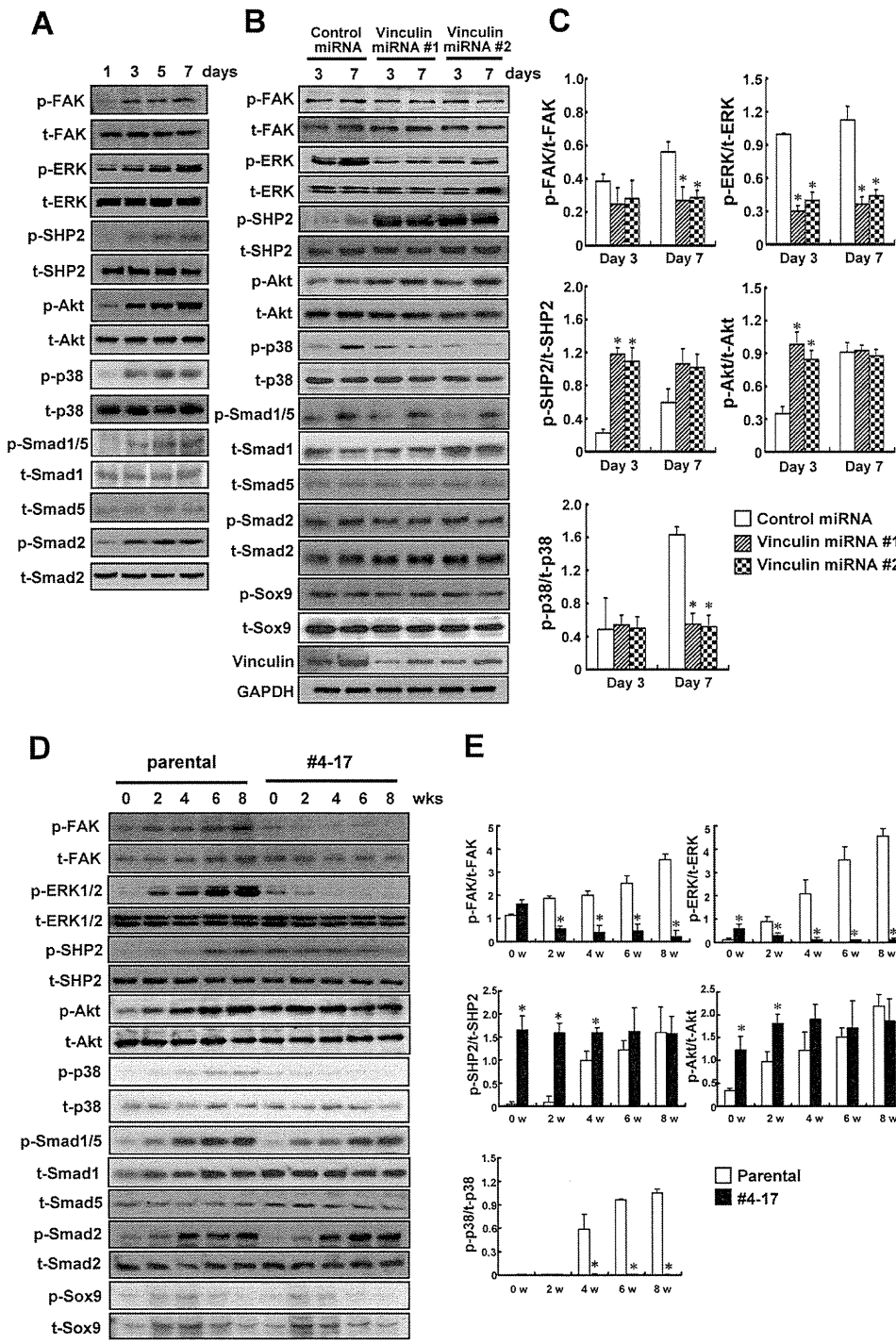

FIGURE 8. **Altered signaling during the chondrocytic differentiation in the cells with a knocked down or trapped vinculin gene.** *A*, increasing phosphorylation of FAK, ERK1/2, SHP2, Akt, p38 MAPK, and Smads during the maturation of primary chondrocytes. *B* and *C*, knockdown of vinculin expression altered the phosphorylation of FAK, ERK1/2, SHP2, Akt, and p38 MAPK during the maturation of primary chondrocytes. Cells were infected with the adenovirus encoding control miRNA or vinculin-specific miRNA on day 1, and lysates were harvested on day 3 and day 7 for Western blotting with the indicated antibodies. The densitometric ratio of the intensity of the signals is demonstrated in *C*. The data are shown as the mean ± S.D. (*error bars*) ($n = 3$). *, $p < 0.05$ *versus* control miRNA. *D* and *E*, phosphorylation status of the signaling molecules during the differentiation of parental ATDC5 cells and clone 4-17 with the trapped vinculin gene. Parental ATDC5 cells and clone 4-17 were cultured in the differentiation medium for the period indicated (0–8 weeks) before lysates were harvested for Western blotting. The densitometric ratio of the intensity of the signals is demonstrated in *E*. The data are shown as the mean ± S.D. ($n = 3$). *p*, phosphorylated; *t*, total; *w*, weeks.

effects of the knockdown of vinculin on chondrogenesis seem to be different from those of β1 integrin or integrin-linked kinase.

Here we applied gene trapping in chondrocytic ATDC5 cells to identify vinculin as involved in chondrocytic differentiation. ATDC5 cells differentiate into mature chondrocytes in several weeks, which enables one to screen the trap clones by phenotype in a relatively short time. On the other hand, gene trapping in ATDC5 cells also has limitations; because the wild-type alleles remain, clones in which some recessive genes are

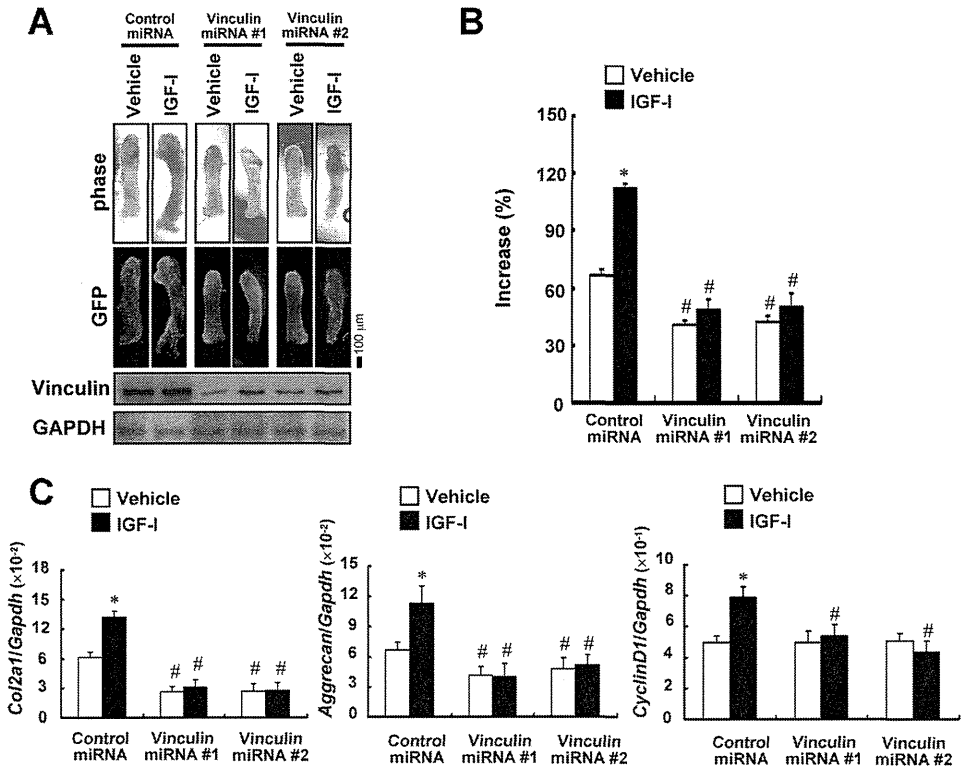

FIGURE 9. **Dysfunctional vinculin caused a disturbance of IGF-I signaling.** *A* and *B*, dysfunctional vinculin impaired the IGF-I-induced growth of metatarsal organ cultures. Metatarsals were infected with the adenovirus encoding control miRNA or vinculin-specific miRNA and treated with 100 ng/ml IGF-I or vehicle for 7 days to evaluate linear growth. Representative images of the phase contrast view and the direct fluorescence of EmGFP derived from the vector-encoding miRNAs are depicted, together with the results of Western blotting. In *B*, the increase in the length of the rudiments is shown as a percentage of the extended length during the culture to the initial length of each bone. The data are shown as the mean ± S.D. (*error bars*) ($n = 3$). *, $p < 0.01$ *versus* vehicle. #, $p < 0.05$ *versus* control miRNA. *C*, dysfunctional vinculin abrogated the IGF-I-induced up-regulation of *Col2a1*, aggrecan, and cyclin D1 expression in the metatarsal organ cultures. RNA was extracted from the metatarsals treated as in *A* and subjected to real-time PCR analyses for the genes indicated.

trapped will be missed in the screening by phenotype. However, when the trapped genes have a dosage effect or the trapping results in a fusion protein with a dominant effect, one can expect the clones to exhibit a unique phenotype in terms of chondrocytic differentiation. In clone 4-17, Western blotting using anti-vinculin antibodies demonstrated that the phenotypical change of the clone was unlikely to be caused by a gene dosage effect (Fig. 1*D*). Instead, we assume that the truncated vinculin derived from the trapped allele has acquired a dominant effect (Fig. 3). The truncated mutant possesses the head domain (Vh) but lacks the tail domain of vinculin (Vt). Wild-type vinculin binds to the integrin-binding protein talin and α-actinin at Vh as well as to actin filaments and paxillin at Vt (25). The conformation of vinculin switches between an inactive "closed" state and an activated "open" state (26–28). In the "closed" state, Vh and Vt bind to each other, masking the binding sites for actin and talin. In the "open" state, Vh can bind to talin and α-actinin, and Vt can bind to actin filaments, thus supporting the linkage between the actin cytoskeleton and integrin adhesion junctions. It was recently reported that the expression of a recombinant Vh domain peptide in smooth muscle tissue inhibited the acetylcholine-induced recruitment of endogenous vinculin to the membrane and the interaction of vinculin with talin and also inhibited vinculin phosphorylation (29). These results indicated that the recombinant Vh peptide inhibited the function of endogenous vinculin. In our study as well, the truncated mutant in clone 4-17 exhibited stronger affinity for talin than did wild-type vinculin, and the mutant appeared to inhibit the interaction between the wild-type vinculin and talin (Fig. 3, *B* and *I*). This inhibition might be a mechanism for the dominant negative effect of the truncated mutant.

In our knockdown experiments, we used gene-specific siRNAs and miRNAs for vinculin. To verify that the effects of vinculin-specific siRNAs and miRNAs were not caused by the suppressed expression of so-called "off-targets," we confirmed that the effects could be cancelled by co-transfection of the vectors encoding the cDNA for wild-type vinculin (Figs. 3*F*, 6 (*A* and *B*), and 7 (*A* and *B*)). Therefore, we prefer to think that the observed effects of the siRNAs and miRNAs were exerted by the decreased expression of vinculin, although we cannot completely exclude the possibility of off-target effects.

Adenoviral transfer of the vinculin-specific miRNA to the metatarsal rudiments markedly reduced the growth and suppressed the expression of *Col2a1* and aggrecan. Because the direct fluorescence of EmGFP in the sections cut from the rudiments demonstrated the viral infection in chondrocytes as well as in perichondrium (supplemental Fig. S4), the suppressed expression of vinculin in chondrocytes was likely to result in the impaired differentiation and the blunted growth of the rudiments. It is possible that the knockdown of vinculin in perichondrium also affected the growth and chondrocyte differentiation by influencing the production of some humoral factors there.

Our results demonstrated that the impaired functioning of vinculin affected multiple signaling pathways involved in chondrocyte differentiation. When primary chondrocytes matured, the phosphorylation of FAK, ERK1/2, SHP2, Akt, p38 MAPK, and Smads was increased, suggesting the involvement of the signaling mediated by these molecules in chondrogenesis (Fig. 8*A*). Activation of ERK1/2 through expression of a constitutively active MEK1 resulted in achondroplasia-like dwarfism in mice (30), indicating the critical role of the MEK/ERK pathway in chondrogenesis. SHP2 encoded by the *PTPN11* gene has been implicated in signal transduction initiated by multiple growth factor and cytokine receptors (31, 32). In humans, mutations in *PTPN11* are responsible for Noonan syndrome and LEOPARD syndrome, characterized by clinical features including skeletal abnormalities (33). As for the PI3K/Akt pathway, studies suggested that it is required for normal hypertrophic cell differentiation and endochondral bone growth (34, 35). In our study, we found that a dysfunctional vinculin affected the MEK/ERK pathway and PI3K/Akt pathway (Fig. 8, *B–E*). Previous studies suggested SHP2 to be a positive regulator in mitogenic signal transduction upstream of ERK1/2 (36, 37). However, the phosphorylation of SHP2 at Tyr-542, which is responsible for the activation of the molecule, was unexpectedly increased by the knockdown of vinculin (Fig. 8, *B* and *C*). It was previously demonstrated that SHP2 was co-immunoprecipitated with vinculin and talin, suggesting that SHP2 associates with the focal adhesion complex (38). Thus, we speculate that the disruption of vinculin interferes with the function of SHP2 in the activation of ERK1/2. Phosphorylation of Akt also has been reported to be regulated by SHP2 (39).

IGF-I is known to regulate the expression of *Col2a1* and aggrecan in chondrocytes via the PI3K/Akt and MEK/ERK pathways (40). Given that the trapping or knockdown of vinculin resulted in the reduced expression of *Col2a1* and aggrecan and affected PI3K/Akt and MEK/ERK signaling, we speculated that the loss of vinculin function reduced the responsiveness of chondrocytes to IGF-I. Consistent with this notion, the IGF-I-induced growth and the up-regulation of *Col2a1* and aggrecan expression were blunted in metatarsal rudiments with the vinculin gene knocked down (Fig. 9), suggesting that vinculin regulates chondrocyte differentiation at least partly through an impact on IGF-I signaling.

Of note, activation of the p38 MAPK pathway in differentiating chondrocytes also was impaired by the loss of vinculin function (Fig. 8, *B–E*). The importance of the p38 MAPK pathway in chondrogenesis was previously suggested by experiments with a transgenic mouse in which a dominant negative form of p38 MAPK was overexpressed in cartilage, resulting in shortened limbs (41). In addition, it was reported that hypoxia induced the expression of *Col2a1* and the production of glycosaminoglycan in a mesenchymal cell line, C3H10T1/2, via activation of the p38 MAPK pathway independently of Sox9 (42). It has also been suggested that p38 MAPK signaling is required for hypertrophic chondrocyte differentiation (43). Considering these observations, the reduced activation of the p38 MAPK pathway also is likely to be responsible for the impaired chondrocytic differentiation caused by the dysfunctional vinculin.

In conclusion, we have demonstrated the tissue-specific function of vinculin in cartilage, by which vinculin controls chondrocytic differentiation. Our results indicate that vinculin has pleiotropic roles in chondrogenesis and regulates the expression of chondrocyte-specific genes via the integration of various signaling pathways. The orchestration of the signaling of humoral factors and the ECM by vinculin appears to be critical to chondrogenesis and should be considered a factor in the regeneration of cartilage.

Acknowledgments—We thank Drs. Noriyuki Tsumaki and Yoshinao Wada for discussions and Dr. Yukinao Shibukawa for technical advice.

REFERENCES

1. Zuscik, M. J., Hilton, M. J., Zhang, X., Chen, D., and O'Keefe, R. J. (2008) Regulation of chondrogenesis and chondrocyte differentiation by stress. *J. Clin. Invest.* **118,** 429–438
2. Kronenberg, H. M. (2003) Developmental regulation of the growth plate. *Nature* **423,** 332–336
3. Stanford, W. L., Cohn, J. B., and Cordes, S. P. (2001) Gene trap mutagenesis. Past, present, and beyond. *Nat. Rev. Genet.* **2,** 756–768
4. Shukunami, C., Shigeno, C., Atsumi, T., Ishizeki, K., Suzuki, F., and Hiraki, Y. (1996) Chondrogenic differentiation of clonal mouse embryonic cell line ATDC5 *in vitro*. Differentiation-dependent gene expression of parathyroid hormone (PTH)/PTH-related peptide receptor. *J. Cell Biol.* **133,** 457–468
5. Ihara-Watanabe, M., Uchihashi, T., Miyauchi, Y., Sakai, N., Yamagata, M., Ozono, K., and Michigami, T. (2004) Involvement of phosphoinositide 3-kinase signaling pathway in chondrocytic differentiation of ATDC5 cells. Application of a gene trap mutagenesis. *J. Cell. Biochem.* **93,** 418–426
6. Uchihashi, T., Kimata, M., Tachikawa, K., Koshimizu, T., Okada, T., Ihara-Watanabe, M., Sakai, N., Kogo, M., Ozono, K., and Michigami, T. (2007) Involvement of nuclear factor I transcription/replication factor in the early stage of chondrocytic differentiation. *Bone* **41,** 1025–1035
7. Jones, P., Jackson, P., Price, G. J., Patel, B., Ohanion, V., Lear, A. L., and Critchley, D. R. (1989) Identification of a talin binding site in the cytoskeletal protein vinculin. *J. Cell Biol.* **109,** 2917–2927
8. Johnson, R. P., and Craig, S. W. (1995) F-actin binding site masked by the intramolecular association of vinculin head and tail domains. *Nature* **373,** 261–264
9. Johnson, R. P., and Craig, S. W. (1995) The carboxyl-terminal tail domain of vinculin contains a cryptic binding site for acidic phospholipids. *Biochem. Biophys. Res. Commun.* **210,** 159–164
10. Turner, C. E., Glenney, J. R., Jr., and Burridge, K. (1990) Paxillin. A new vinculin-binding protein present in focal adhesions. *J. Cell Biol.* **111,** 1059–1068
11. Xu, W., Coll, J. L., and Adamson, E. D. (1998) Rescue of the mutant phenotype by reexpression of full-length vinculin in null F9 cells. Effects on cell locomotion by domain-deleted vinculin. *J. Cell Sci.* **111,** 1535–1544
12. Xu, W., Baribault, H., and Adamson, E. D. (1998) Vinculin knockout results in heart and brain defects during embryonic development. *Development* **125,** 327–337
13. Coll, J. L., Ben-Ze'ev, A., Ezzell, R. M., Rodríguez Fernández, J. L., Baribault, H., Oshima, R. G., and Adamson, E. D. (1995) Targeted disruption of vinculin genes in F9 and embryonic stem cells changes cell morphology, adhesion, and locomotion. *Proc. Natl. Acad. Sci. U.S.A.* **92,** 9161–9165
14. Volberg, T., Geiger, B., Kam, Z., Pankov, R., Simcha, I., Sabanay, H., Coll, J. L., Adamson, E., and Ben-Ze'ev, A. (1995) Focal adhesion formation by F9 embryonal carcinoma cells after vinculin gene disruption. *J. Cell Sci.* **108,** 2253–2260
15. Lefebvre, V., Garofalo, S., Zhou, G., Metsäranta, M., Vuorio, E., and De Crombrugghe, B. (1994) Characterization of primary cultures of chondrocytes from type II collagen/β-galactosidase transgenic mice. *Matrix Biol.*